

Review

# Gas-Phase Oxidative Dehydrogenation of *n*-Octane over Metal Oxide Catalysts: A Review

Pinkie Ntola <sup>1,\*</sup>  and Mzamo Shozi <sup>2,\*</sup> <sup>1</sup> Department of Chemistry, Durban University of Technology, P.O. Box 1334, Durban 4000, South Africa<sup>2</sup> School of Chemistry and Physics, University of KwaZulu-Natal, Private Bag X54001, Durban 4000, South Africa

\* Correspondence: pinkies@dut.ac.za (P.N.); shozim2@ukzn.ac.za (M.S.)

**Abstract:** The oxidative dehydrogenation (ODH) of alkanes, whereby hydrogen is removed to form unsaturated compounds, is an important process, particularly in the petrochemical industry. The ODH of lighter alkanes (C3–C6) is well-reported in the literature, and while there are several reports on the ODH of *n*-octane (C8), there is no reported review of the important findings in the literature. This review discusses the gas-phase ODH of *n*-octane occurring at high temperatures (300–550 °C). The mechanisms via which the *n*-octane ODH occurs are also briefly discussed. The oxidants (mainly O<sub>2</sub> and CO<sub>2</sub>) and catalysts (supported and unsupported metal oxides) are discussed as well as the effect of these and the temperature on the type of products formed and their various distributions. Furthermore, the review looks at the acid–base and redox properties of the catalysts and how they affect product formation. Some challenges as well as perspectives of the ODH process are also highlighted.

**Keywords:** *n*-octane; oxidative dehydrogenation; metal oxides; oxidants



**Citation:** Ntola, P.; Shozi, M. Gas-Phase Oxidative Dehydrogenation of *n*-Octane over Metal Oxide Catalysts: A Review. *Catalysts* **2024**, *14*, 100. <https://doi.org/10.3390/catal14020100>

Academic Editors: Andrea Goti and Camilla Matassini

Received: 1 January 2024

Revised: 19 January 2024

Accepted: 23 January 2024

Published: 25 January 2024



**Copyright:** © 2024 by the authors. Licensee MDPI, Basel, Switzerland. This article is an open access article distributed under the terms and conditions of the Creative Commons Attribution (CC BY) license (<https://creativecommons.org/licenses/by/4.0/>).

## 1. Introduction

### 1.1. Importance of Alkane Activation and Associated Products

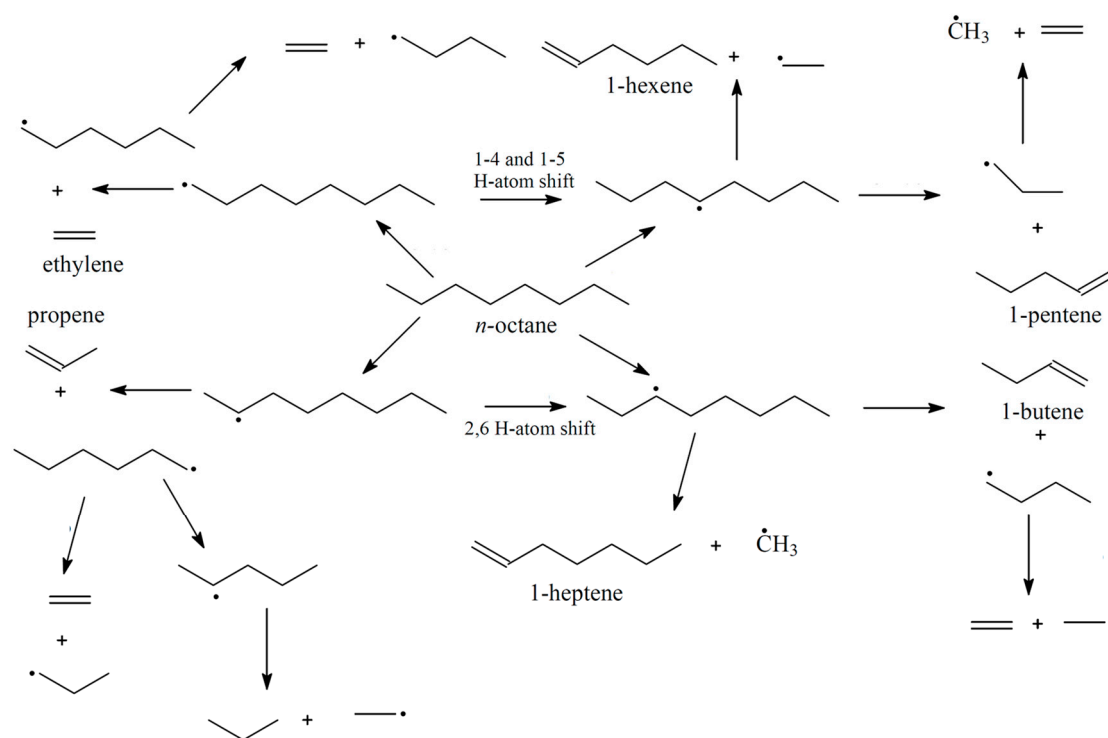
C–H bond activation has been studied for decades with particular attention to the selective transformation of inert carbon–hydrogen bonds into other useful functional groups more recently. The conversion of long-chain and medium-chain alkanes to value-added products is an important reaction both industrially and scientifically, as the low octane number *n*-alkanes get converted into the high octane number alkenes, dienes, and aromatics [1,2]. Over the span of many years, research has shown that there is an increased demand for alkenes, aromatic compounds and functionalized alkanes, which can be derived from alkanes as feedstock. Alkenes constitute highly adaptable intermediates for the manufacture of many value-added chemicals [3]. Medium-chain olefins are majorly used in the synthesis of alcohols or aldehydes, the production of copolymers with short-chain olefins and the production of synthetic lubricants [4,5]. With regards to aromatics, despite the growing interest in biofuels, especially renewable hydrocarbon, the current process for hydrocarbon production still lacks a step for producing aromatics. Aromatics are important as they increase the octane rating in bio-gasoline and give solvent characteristics in the fuel [6]. These compounds are also useful in the improvement of the anti-knock index in petroleum fuels. Table 1 summarizes the main uses of alkenes obtained from the oxidation of long- and medium-chain alkanes [7].

**Table 1.** Main uses of alkenes [7].

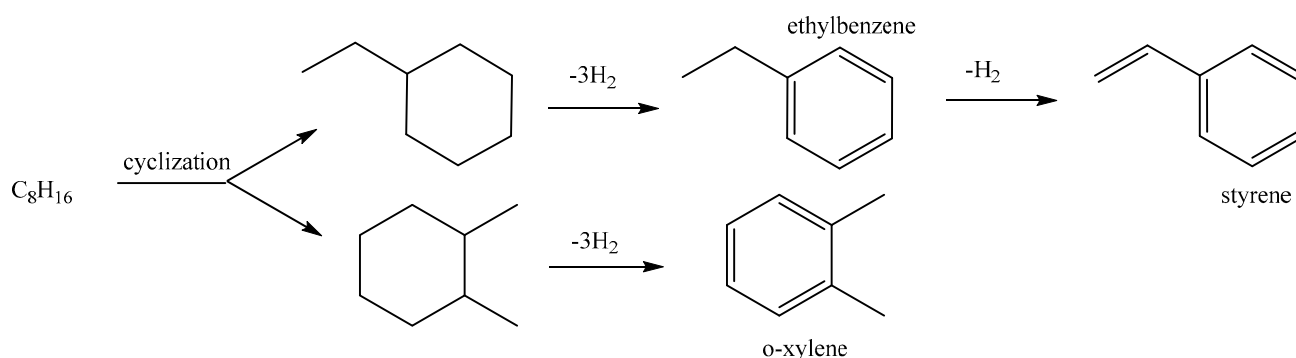
Ethene	Polymers (PE), ethylene oxide, vinyl acetate, vinyl chloride, styrene
Propene	Propene polymers (PP), propene oxide, acetone, butanal, plasticizer alcohols, acrylonitrile, epichlorohydrin synthesis
1-Butene	Butene polymers, solvents
Butadiene	Polymers, oligomers, adiponitrile, sulfolane, chloroprene, vinylcyclohexene, cyclododecatriene
1-Hexene	Co-monomer in PE
1-Heptene	Reagent and solvent in organic synthesis
1-Octene	Co-monomer in PE
C10-C14	Detergent alcohols
C14-C16	Sulfates and sulfonates in detergents

### 1.2. Conversion of Intermediate Chain Alkanes

Linear alpha olefins/1-alkenes were initially produced from paraffinic wax using thermal cracking. This process gave a large proportion of 1-alkenes as the primary products, together with alkanes [8]. Products such as detergent alcohols could be produced subsequently via the hydro formylation of mixtures of 1-alkenes and internal alkenes. C4–C8 linear alpha olefins are majorly used for producing linear aldehydes via oxosynthesis for the later production of fatty acids. This is achieved via oxidation of the intermediate aldehydes, or linear alcohols for plasticizer applications [9,10]. Industrially, alkenes are produced following dehydrogenation (cracking) of alkanes at extremely high temperatures (500–900 °C), which results in high energy consumption. However, the dehydrogenation of alkanes to olefins and hydrogen is an endothermic process limited by the thermodynamic equilibrium. There are basically two undesirable features of the dehydrogenation reaction, viz., high energy consumption and the breaking of the equilibrium while the equilibrium limitation is also broken [11]. As such, researchers have shown an interest in the conversion of alkanes using various oxidants. These reactions have shown higher conversion and low carbon deposition with a lower energy demand than the non-oxidative route [12]. While the dehydrogenation of short-chain (C2–C4) and long-chain paraffins (C10–C14) has been studied vastly, there are very limited studies on the conversion of n-paraffins with intermediate chain length (C6–C9) to linear olefins. Scheme 1 shows the various reaction pathways as well as the possible products that can be obtained from the oxidation of *n*-octane at 530 °C. These pathways were proposed by Sarathy et al. [13], and the radicals and intermediate products formed may react further to form products not shown, such as octenes and subsequently aromatics. Scheme 2 shows the reaction pathway for the cyclization of the formed octenes to produce aromatics. Despite the advantages offered by the ODH route, there are difficulties with respect to converting *n*-octane in particular.



**Scheme 1.** Reaction pathways for *n*-octane oxidation as proposed by Sarathy et al. [13].



**Scheme 2.** The pathway for the formation of aromatics from formed octenes via ODH and cyclization. Adapted from Széchenyi and Solymosi [14].

### 1.3. Challenges Associated with Converting *n*-Octane to Value-Added Products

Transition metal-catalyzed dehydrogenation reactions have become popular and attractive due to the increasing demand for sustainable oxidation methods. However, these methods usually apply hazardous and environmentally unfriendly oxidants [1]. Using milder oxidants such as molecular oxygen, carbon dioxide and hydrogen peroxide as an environmentally friendly alternative has proven to solve the problems associated with over-oxidation [15]. Amongst the various challenges faced with the conversion of alkanes is the potentially dangerous fuel/oxidant mixtures that must be monitored. Also, while many researchers have demonstrated that the ODH of paraffins in the presence of molecular oxygen in particular resulted in a higher conversion, less carbon deposition and a lower demand of energy compared to the non-oxidative route, it showed low selectivities to olefins [16,17]. The use of molecular oxygen ( $O_2$ ) has the propensity to complicate the reaction, in that activated electrophilic oxygen species are formed, which tend to attack a region of high electron density, such as the double bond of an alkene. This results in the formation of epoxy or peroxy species, leading to the breakdown of the hydrocarbon skeleton of alkenes and the feed alkane (Figure 1). This results in the formation of thermodynamically

stable CO<sub>2</sub> and water [18,19]. Therefore, the main challenge in the ODH of alkanes is that the total oxidation products (carbon oxides) are thermodynamically more stable than the dehydrogenation products, which are olefins and aromatics. Designing catalysts that can enable the reaction to stop at intermediate stages (to enable the formation of olefins and aromatics) remains a challenge. For the production of aromatics, hydrogenolysis and deactivation form part of the challenge. A number of reviews have been published on the oxidative dehydrogenation of shorter and medium-chain alkanes. Despite the recent short review on the oxidation of *n*-alkanes on various catalysts and C-H bond activation by Isazade [20], there is still very limited literature on *n*-octane activation in particular. This review provides an overview of the challenges and current trends with respect to the types of catalysts used, the oxidants, suggested mechanisms and perceptions.

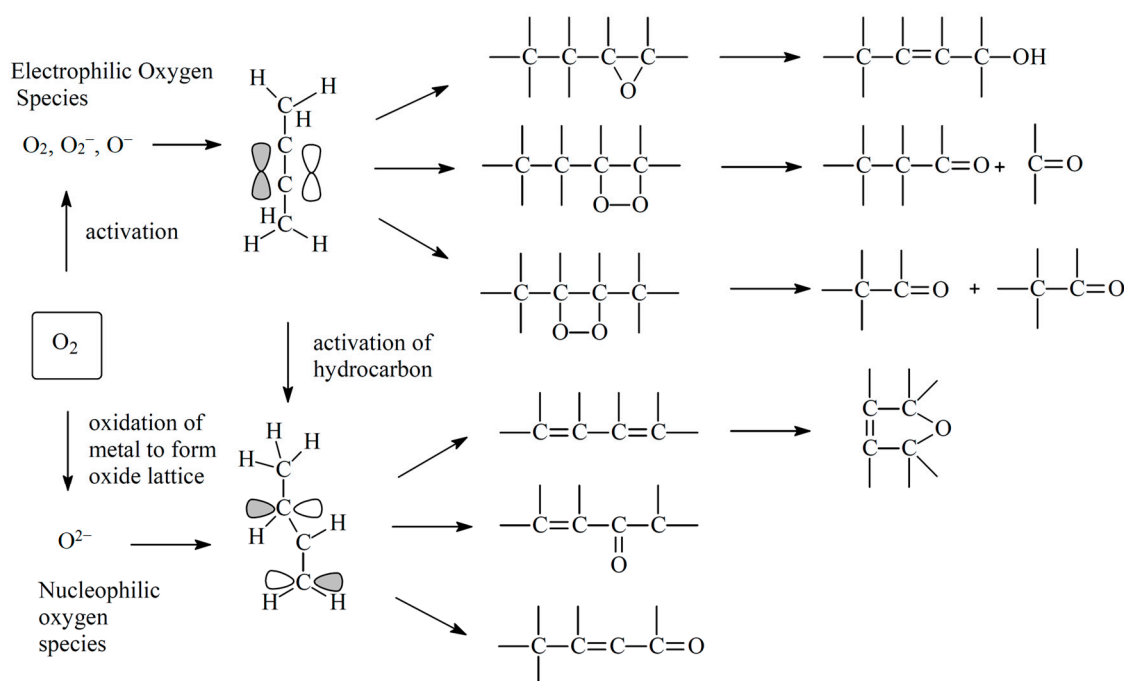


**Figure 1.** Mechanism of catalytic oxidation of alkanes. Reproduced from [21].

## 2. Oxidants

Despite molecular oxygen being the most studied oxidant in the oxidative dehydrogenation of alkanes, there are other oxidants such as CO<sub>2</sub>, bromine, sulphur, N<sub>2</sub>O and iodine and their compounds. These oxidants offer the advantage of high selectivity for dehydrogenation. However, halogen and sulfur gases are corrosive and are a potential environmental concern, which has deterred their commercialization [22]. N<sub>2</sub>O and CO<sub>2</sub> are regarded as unconventional oxidants (as opposed to molecular oxygen). However, due to the different nature of the oxygen species they generate and their lower oxidizing power, they are used to evade the selectivity issue encountered when molecular oxygen is used [23]. Nonetheless, for the oxidative dehydrogenation of *n*-octane, the use of oxidants is mainly limited to molecular oxygen and CO<sub>2</sub>.

### 2.1. Molecular Oxygen

The oxidative dehydrogenation route to activating alkanes provides the advantage of low environmental impact and a relatively low cost of raw materials. Using molecular O<sub>2</sub> in the reaction allows for oxidative dehydrogenation over properly selected catalysts, which can produce oxygenated compounds [24]. In the case of molecular oxygen as an oxidant, it has been demonstrated that many metal oxides have different abilities to activate O<sub>2</sub>, and the metal oxide's tendency to activate O<sub>2</sub> depends on its ability to chemisorb O<sub>2</sub> [25,26]. The various properties that determine the ability of metal oxide catalysts to activate oxygen

include the rate and extent of reduction, the electronic properties and the surface acidity, bandgap energy of the metal oxides and O<sub>2</sub> activation.

Fadlalla and Friedrich studied the oxidative dehydrogenation of *n*-octane using cobalt molybdate catalysts under varying oxygen ratios. The results indicated that under dehydrogenation conditions, the catalyst demonstrated low *n*-octane conversion, which resulted in the complete segregation of the catalyst. Additionally, the introduction of oxygen showed a notable improvement in the conversion and also the selectivity to aromatics. Different C-to-O<sub>2</sub> ratios gave different selectivity profiles. The best carbon-to-oxygen ratio for octenes was an 8:1 C:O ratio, while for aromatics it was 8:3 [27].

## 2.2. Carbon Dioxide

Carbon dioxide can be used as a soft oxidant in the ODH of alkanes (CO<sub>2</sub>-ODH). The use of CO<sub>2</sub> is regarded as beneficial since it can be re-used and meet the demand for olefins [28]. Using CO<sub>2</sub> as an oxidant is a greener alternative to the traditional dehydrogenation process [29–32]. The use of CO<sub>2</sub> can also be regarded as an attractive route when it comes to CO<sub>2</sub> mitigation via carbon capture and use [33]. Various authors have used different materials to activate CO<sub>2</sub> and, in some cases, indicated the role CO<sub>2</sub> played as an oxidant. In a study conducted by Adam et al., the role of CO<sub>2</sub> as an oxidant was investigated during the dehydrogenation of *n*-octane using Cr-Fe catalysts. The CO<sub>2</sub>-ROR and EPR results demonstrated that CO<sub>2</sub> performed an oxidative role over the Cr monometallic catalyst. Adam et al. used a reaction mechanism to illustrate that the predominant mechanism over the Cr catalyst used is via the CO<sub>2</sub>-ODH (Figure 2) [31].

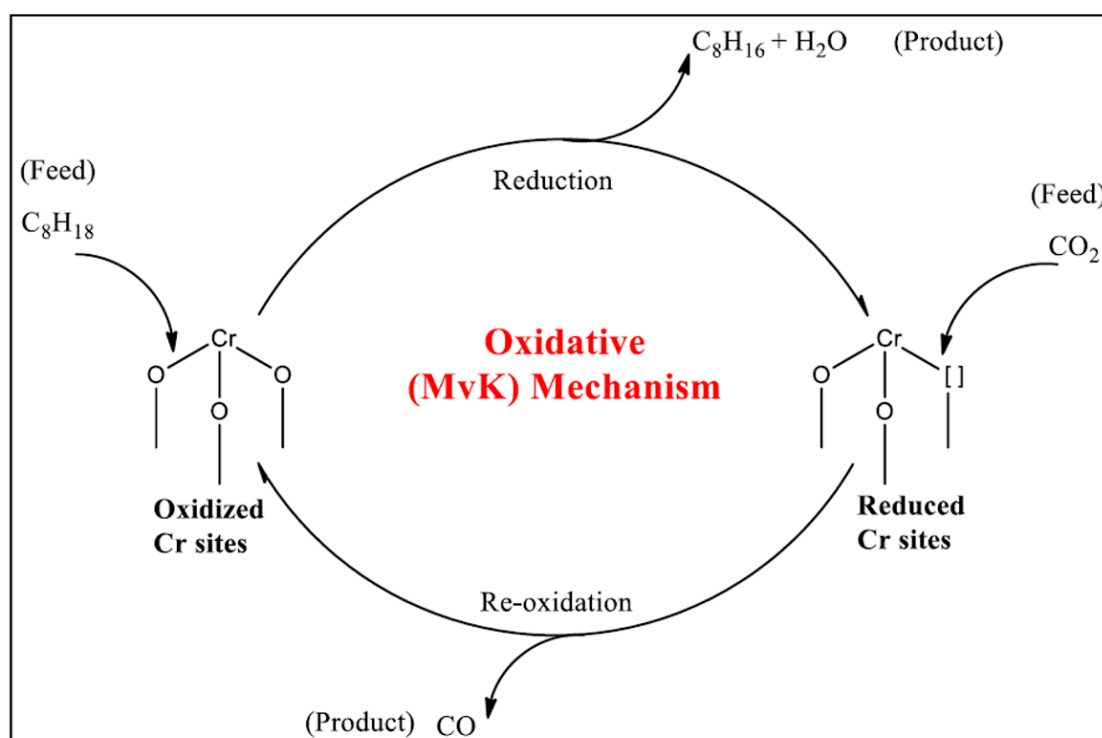


**Figure 2.** The oxidative dehydrogenation (ODH) mechanism for CO<sub>2</sub> activation of *n*-octane over the Cr monometallic catalyst. Reprinted from [31] with permission from Elsevier.

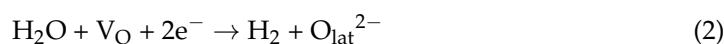
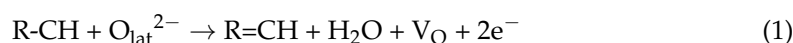
Moloi et al. [30] investigated the CO<sub>2</sub>-assisted activation of *n*-octane over VO<sub>x</sub> supported on anatase catalysts that showed superior interaction with CO<sub>2</sub> by dissociating it. This was followed by lattice oxygen replenishment by the oxygen reduced. During CO<sub>2</sub> dissociation, the oxygen produced may replenish lattice oxygen, which may then react with hydrogen via the reverse water gas shift reaction. Additionally, a combustion of carbon deposits may occur via the reverse Boudouard reaction. Another study conducted

by Farahani et al. where mesoporous 2D NiO–Nb<sub>2</sub>O<sub>5</sub>–Al<sub>2</sub>O<sub>3</sub> and template-free ordered mesoporous alumina were used in a CO<sub>2</sub>-assisted dehydrogenation of an *n*-octane reaction gave more insights about the role of CO<sub>2</sub> in the reaction. The results obtained showed that adding Nb<sub>2</sub>O<sub>5</sub> to the NiO catalyst facilitates CO<sub>2</sub>-DH via the promotion of the RWGS and reverse Boudouard reactions. This was consistent with the findings of Moloi et al., even though the two studies employed different catalytic systems. Despite the limited use of this oxidant in the dehydrogenation of *n*-octane, previous studies on shorter chain alkanes, such as butane, and theoretical studies have demonstrated that CO<sub>2</sub> has a kinetic barrier, and its activation energy is higher than that of O<sub>2</sub> and N<sub>2</sub>O [34,35]. An important factor to consider in the ODH of alkanes is the mechanism that describes the kinetics of the reactions, their positions and limitations.

### 3. Mechanisms of Alkane Oxidation

#### 3.1. Mars and Van Krevelen

This mechanism was developed by Mars and Van Krevelen when they investigated naphthalene oxidation [36]. It was developed for oxidation reactions where the catalysts are based on transition metal oxides which are able to change their oxidation states easily [37]. The mechanism is reported by Hosono et al. [38] to occur via the following reactions:



In the above reactions, O<sub>lat</sub><sup>2-</sup> and V<sub>O</sub> represent the lattice oxygens and oxygen vacancies, respectively. Figure 3 shows a schematic diagram of the Mars van Krevelen (MvK) mechanism proposed by Pan et al. [39]. In this mechanism, the alkane (R<sub>H</sub>) is activated by the lattice oxygen from the metal oxide catalyst to form the oxidative product (R<sub>O</sub>), resulting in oxygen vacancies. The catalyst is re-oxidized by the oxygen adsorbed on the catalyst surface, thereby replenishing the oxygen vacancies. Water and carbon dioxide are the main by-products of this process.

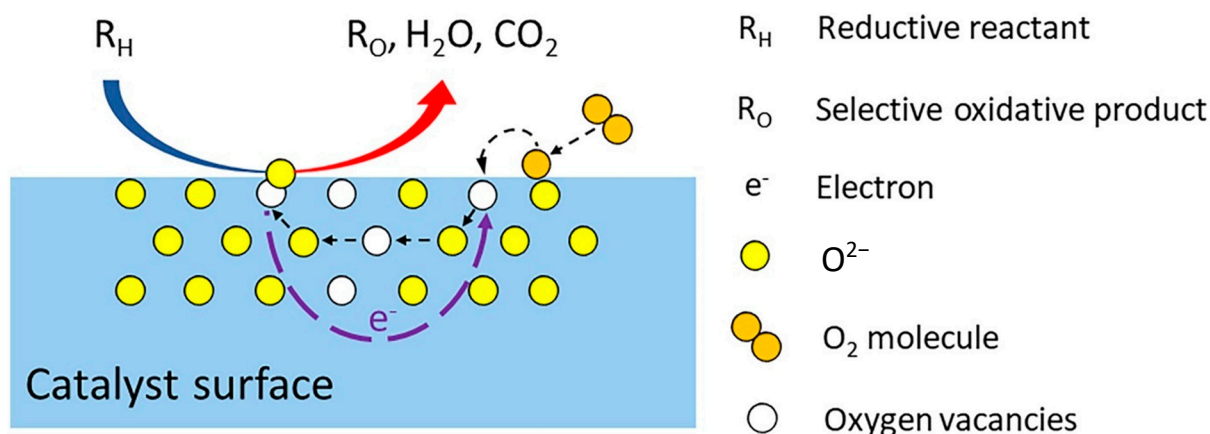


**Figure 3.** Schematic diagram of the Mars van Krevelen mechanism. Reproduced from [39].

#### 3.2. Langmuir–Hinshelwood and Eley–Rideal

The Langmuir–Hinshelwood (LH) mechanism finds applications in reactions where organic substrates undergo oxidation on the catalyst surface in the presence of oxygen [40]. The mechanism assists in explaining the kinetics between two adsorbed species and assumes that the energy of interaction between the adsorbent and adsorbate is constant as the coverage increases. On the other hand, in the Eley–Rideal (ER) mechanism, one of the species is adsorbed on the catalyst surface, and the other species reacts with the chemisorbed species in the gas phase [41]. The Eley–Rideal mechanism is not as common as the Langmuir–Hinshelwood mechanism, and the majority of surface-catalyzed reactions

are said to follow the latter mechanism. Figure 4 shows a diagrammatic representation of both the LH and ER mechanisms [42].

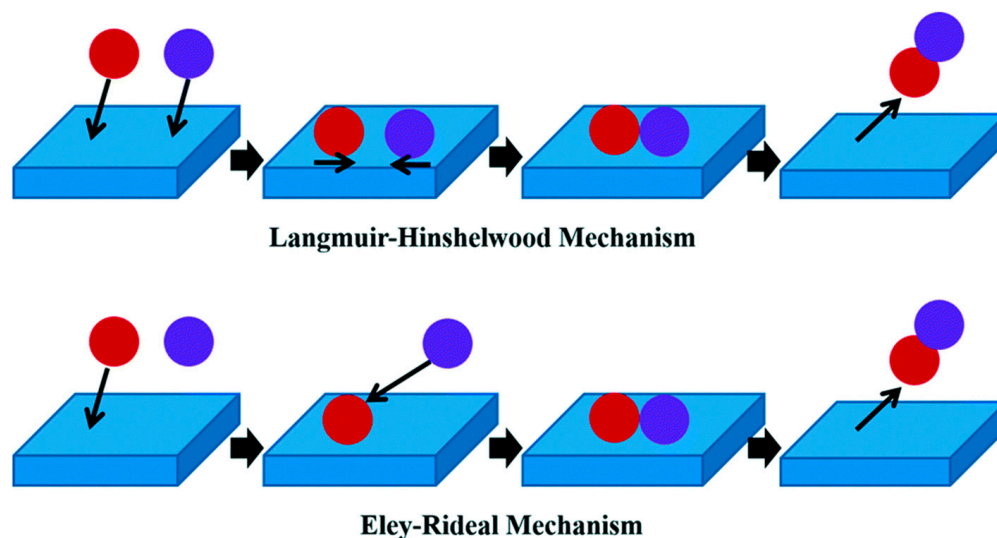


**Figure 4.** Schematic diagram of the Langmuir–Hinshelwood and Eley–Rideal mechanisms. Used with permission from the Royal Society of Chemistry, from [42]; permission conveyed through Copyright Clearance Center, Inc.

It is, however, important to note that the mechanisms depend on the catalysts used.

#### 4. Catalysts Used

A variety of classes of catalysts have been employed for the ODH of *n*-octane. These include unsupported metal oxides [43–46], supported metal oxides [47–52], mixed metal oxides, zeolites [53,54] and hydroxyapatites [24,55–57]. This review focuses on unsupported and supported metal oxides. Properties of metal oxides catalysts can be tuned to achieve improved selectivities towards the sought products [45]. It has been shown that the formation of active oxygen species during the re-oxidation of the catalysts influences the selectivity of products in the oxidative dehydrogenation of *n*-octane. Mechanistic investigations have revealed that the basicity and the redox capacity of the metal will influence the selectivity to olefins [55,58]. Metal oxides interact with the hydrogen atoms of alkanes and promote the dissociation of C–H bonds and the subsequent formation of hydrogen and olefins. Bulk metal oxides generally possess low surface areas and large crystallite sizes. These also present low activity and are prone to deactivating rapidly due to sintering [59]. Metal oxides used for the activation of paraffins may be unsupported, supported and or mixed.

##### 4.1. Unsupported Metal Oxides

Metal oxides have been widely explored as catalysts in the oxidative dehydrogenation of *n*-octane. Some common unsupported metal oxide catalysts are those based on vanadium, chromium and iron. Friedrich and Mahomed [60] reported the use of an Mg–V hydrotalcite-like catalysts synthesized via a coprecipitation method, in the oxidative dehydrogenation of *n*-octane to styrene. Figure 5 shows the selectivity and yield of styrene obtained over a temperature range of 300–550 °C. The *n*-octane conversion increased with increasing temperature, and the formation of styrene was observed from 400 °C. The selectivity to styrene increased up to 500 °C and thereafter decreased. Other products obtained were olefins, oxygenates, cracked products and carbon oxides.

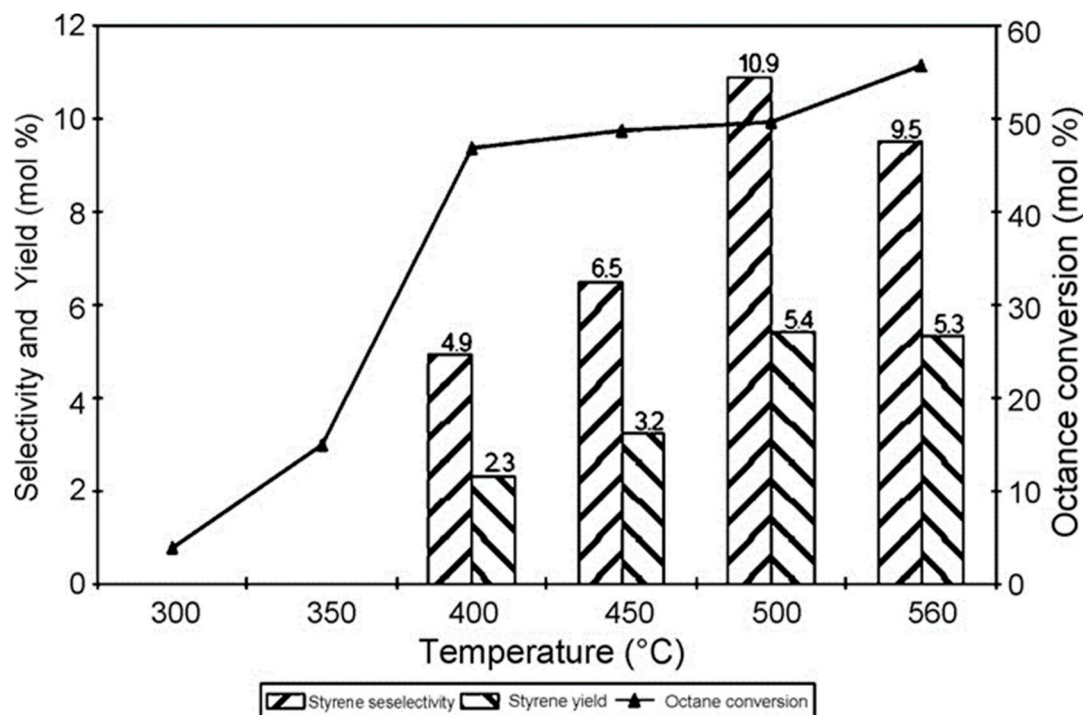


**Figure 5.** Effect of temperature on octane conversion, styrene selectivity and yield (Mg–V, 7% octane in air, GHSV = 3440 h<sup>-1</sup>). Reprinted from [60] with permission from Elsevier.

Narayanappa et al. [61] reported the use of a cobalt-substituted ceria catalyst synthesized via a single-step solution combustion method. They investigated the effect of temperature and the *n*-octane-to-oxygen feed ratio on the octane and oxygen conversion (Figure 6) and product formation (Figure 7) over Ce<sub>0.90</sub>Co<sub>0.10</sub>O<sub>2-δ</sub>. In Figure 6, an apparent increase in both the octane and oxygen conversion with an increase in temperature can be observed over all octane-to-oxygen-feed ratios. The increase in octane conversion was reported to be due to the bulk reduction of Co<sup>3+</sup> as the temperature increased. The resulting Co<sup>2+</sup> ions formed defect centers which formed oxygen vacancies, aiding in the oxidation. The increase in oxygen conversion (Figure 6b) showed that the reaction proceeded under aerobic conditions, and it was assumed that the reaction was mainly oxidative.

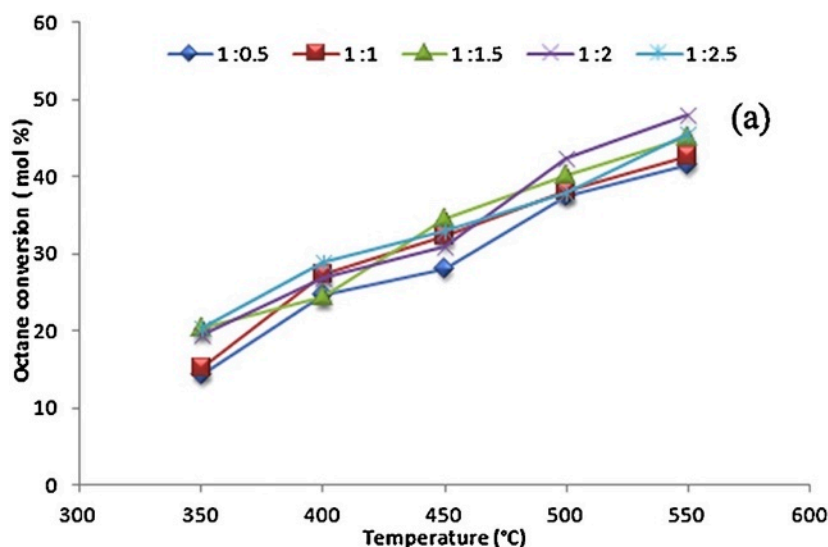


**Figure 6.** Cont.

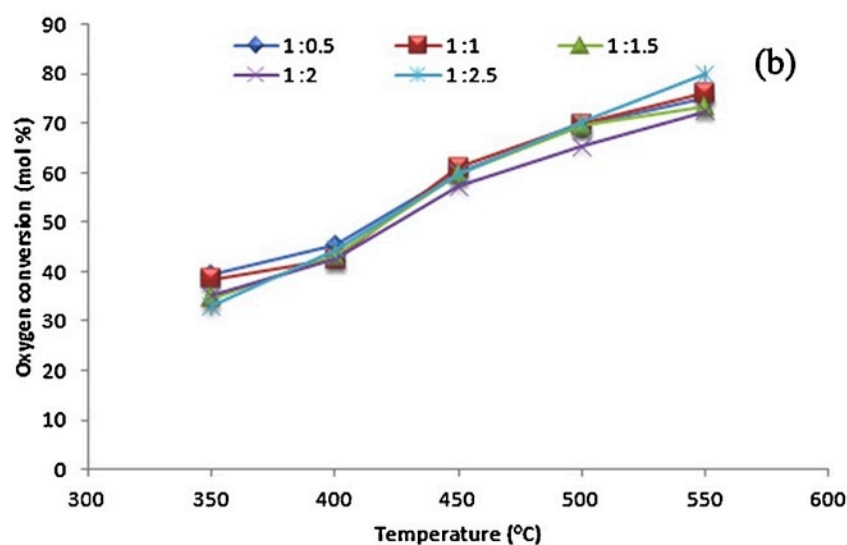


**Figure 6.** Effect of temperature on octane conversion (a) and oxygen conversion (b) over  $Ce_{0.90}Co_{0.10}O_{2-\delta}$  at various *n*-octane-to-oxygen feed ratios (GHSV = 4000 h<sup>-1</sup>). Reproduced from [61] © 2012, with permission from Elsevier.

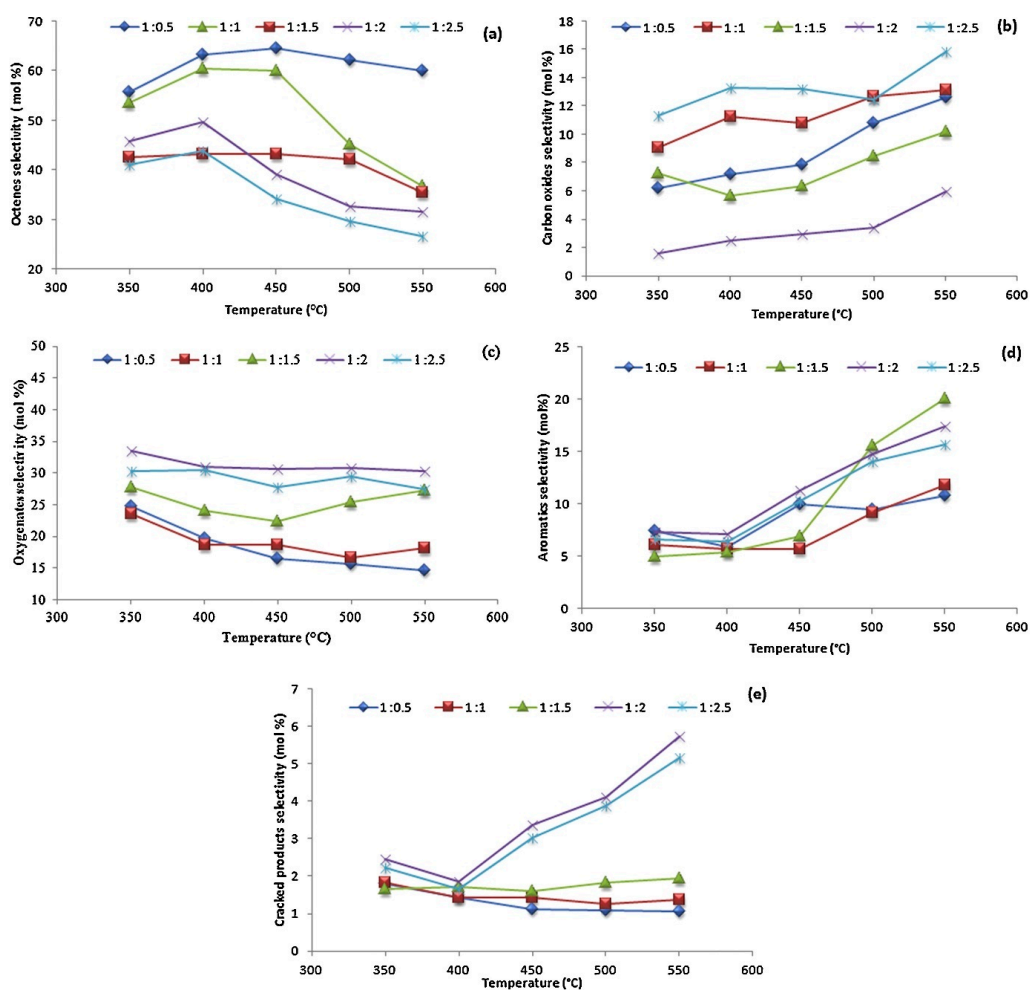


**Figure 7.** Product selectivity (a) octenes, (b) carbon oxides, (c) oxygenates, (d) aromatics and (e) cracked products over  $Ce_{0.90}Co_{0.10}O_{2-\delta}$  at various temperatures and *n*-octane-to-oxygen feed ratios. Reproduced from [61] © 2012, with permission from Elsevier.

Figure 7 shows the product selectivity over  $\text{Ce}_{0.90}\text{Co}_{0.10}\text{O}_{2-\delta}$  at various temperatures and *n*-octane-to-oxygen-feed ratios. Octenes were the major products at lower octane-to-oxygen-feed ratios. It was believed that this was due to the limited oxygen supply favoring the dehydrogenation of octane through reducing  $\text{Co}^{3+}$  to  $\text{Co}^{2+}$  in the catalyst. The octene selectivity, however, decreased at ratios higher than 1:1.5 and higher temperatures at the expense of the formation of oxygenates, aromatics, carbon oxides (CO and  $\text{CO}_2$ ) and cracked products. The selectivity to carbon oxides (Figure 7b) was fairly constant up to a ratio of 1:1.5. At higher ratios, an increase in  $\text{CO}_2$  was reported to be due to the oxide ion vacancy in the metal lattice as  $\text{Co}^{2+}$  was oxidized to  $\text{Co}^{3+}$  under strong oxidizing conditions. These oxide ions promoted the formation of  $\text{CO}_2$  via the secondary oxidation of CO. The formation of aromatics increased above 450 °C with a simultaneous decrease in octenes, since the production of aromatics from octenes was favored under dehydrogenative conditions and high temperature [31].

Fadlalla and Friedrich [27] investigated the effect of temperature and the carbon-to-oxygen ratio on the activity and selectivity to aromatics and octenes over cobalt molybdate in the oxidative dehydrogenation of *n*-octane. Figure 8 shows the *n*-octane conversion and general product selectivity over cobalt molybdate from 350 to 550 °C. In Figure 8a, it can be seen that the conversion was low, reaching a maximum of 11% at 550 °C. This was attributed to a lack of formation of carbon oxides and water and resulted in the equilibrium not being pushed toward product formation. Trans-2-octene was the dominant product amongst the octenes (Figure 8b), whilst xylene was the dominant product amongst the aromatics (Figure 8c). It was suggested that xylene is produced from trans-2-octene via a 2,7-cyclization mechanism. The absence of 1-octene was attributed to the presence of ethylbenzene and styrene, as this highly reactive olefin is believed to form these aromatics via a 1,6-cyclization mechanism.

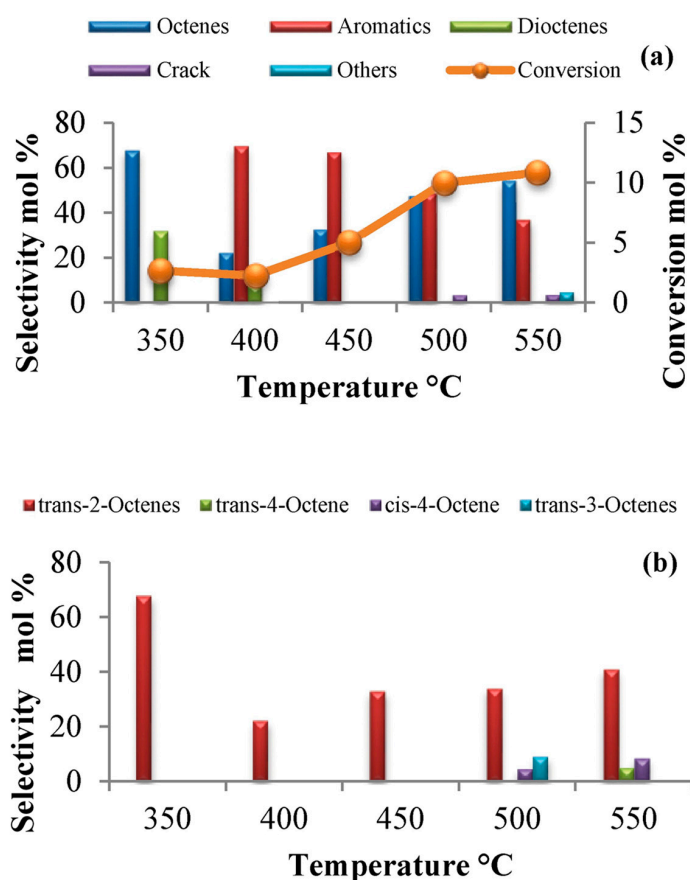
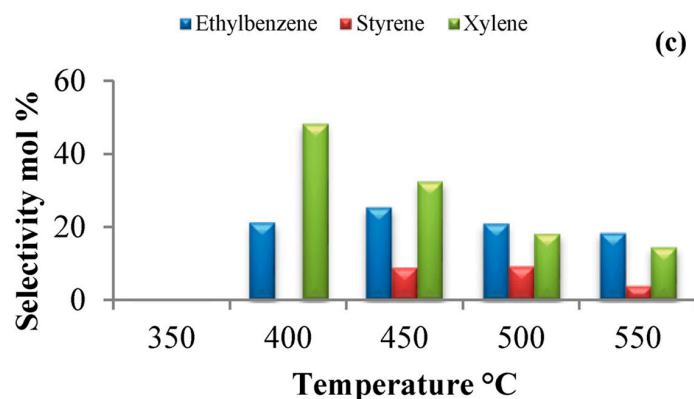
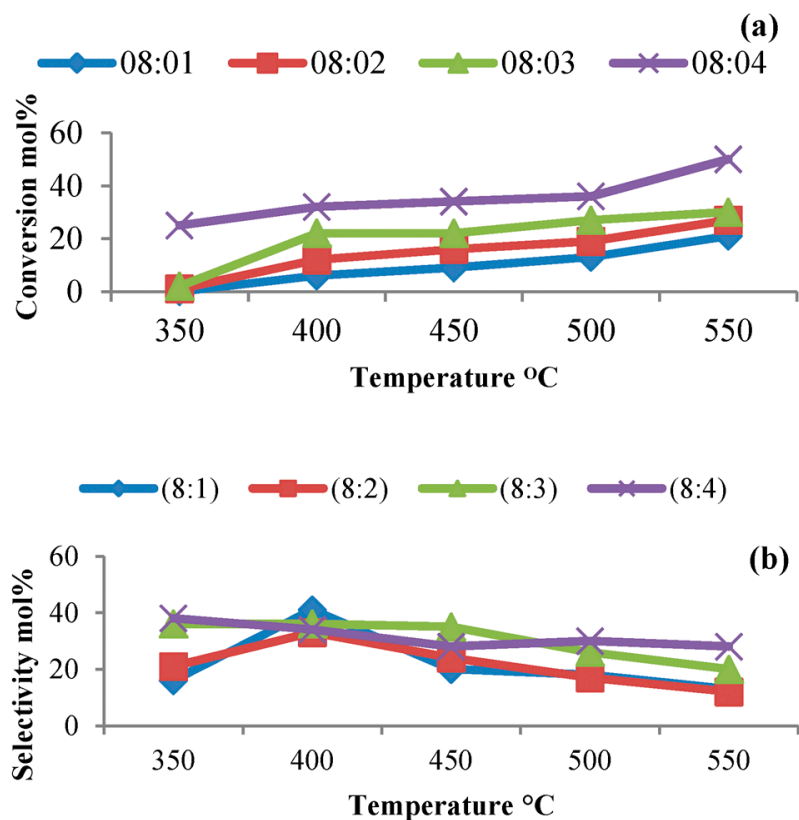


Figure 8. Cont.



**Figure 8.** *n*-Octane conversion and general product selectivity mol% (a), octenes selectivity mol% (b), and aromatics selectivity mol% (c), breakdown over cobalt molybdate at C:O ratio = 8:1 and GHSV = 4000 h<sup>-1</sup>. Used with permission from the Royal Society of Chemistry, from [27]; permission conveyed through Copyright Clearance Center, Inc.

To investigate the effect of the carbon-to-oxygen ratio on activity and product selectivity, four different C:O ratios were chosen at temperatures 350–550 °C (Figure 9). The conversion increased with increasing C:O ratios (Figure 9a). There was an increase in selectivity to carbon oxides up to 400 °C, and thereafter, it decreased. This was attributed to the formation of oxidative dehydrogenation products. The selectivity to octenes was favored at low C:O ratios and compared to higher ratios where secondary reactions took place converting these octenes into aromatics and cracked products. This is supported by the data observed in Figure 9d where a general increase in aromatics is observed over all C:O ratios, due to the cyclization mechanisms of formed octenes.



**Figure 9.** Cont.

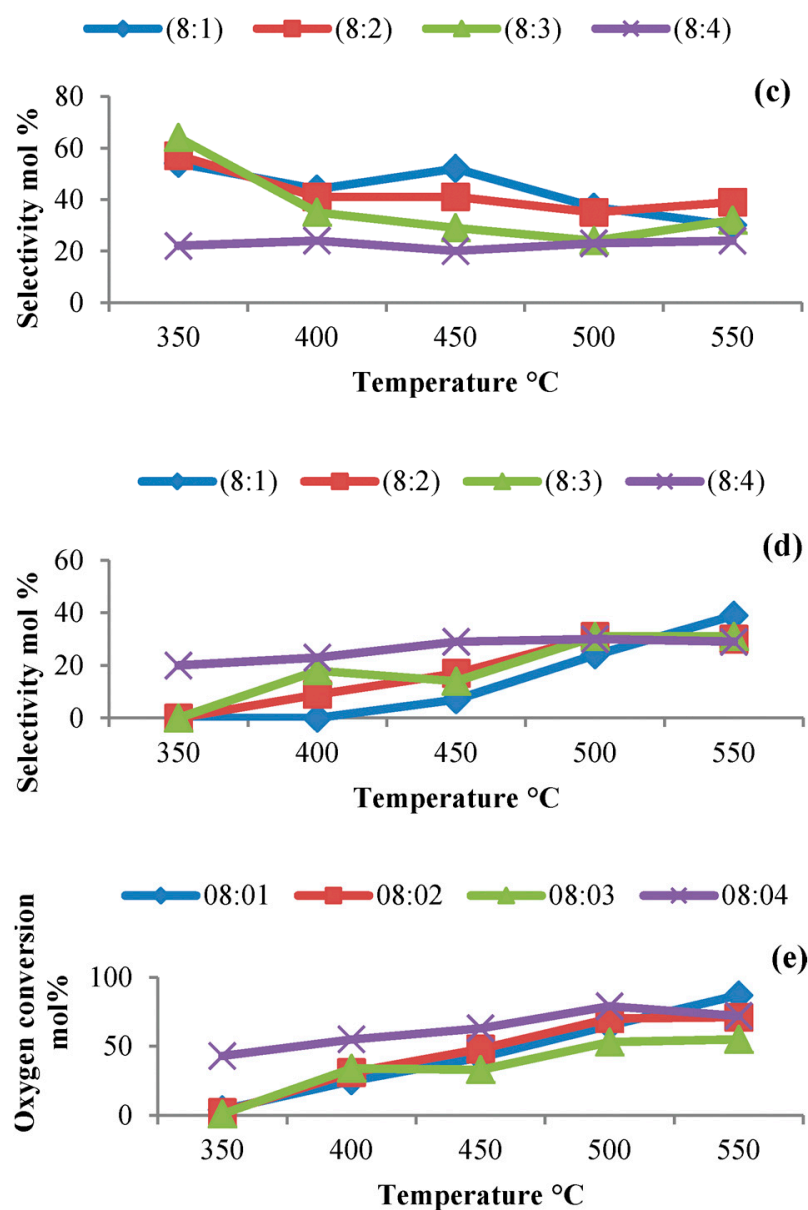


**Figure 9.** Effect of temperature and C:O ratio on *n*-octane conversion (a), CO<sub>x</sub> selectivity (b), octenes selectivity (c), aromatics selectivity (d) and oxygen conversion (e) over cobalt molybdate (GHSV = 4000 h<sup>-1</sup>). Used with permission from the Royal Society of Chemistry, from [27]; permission conveyed through Copyright Clearance Center, Inc.

Hydroxyapatites (HAp) are amphoteric in nature and highly stable, and the phosphate groups in the structure are able to activate oxygen, making them suitable catalysts and supports in alkane oxidative dehydrogenation [62,63]. The combined acidity of the phosphate groups and the alkali earth metal create active sites which are capable of activating oxygen, resulting in oxygen species that are able to abstract hydrogen in alkanes [64]. Dasireddy et al. [56] reported the use of alkali earth metal hydroxyapatites in the oxidation of *n*-octane. The conversion increased with an increase in temperature, which was reported to be due to the surface oxygen species chemisorbed on the catalyst (Figure 10). Redox properties of the catalysts did not contribute to the conversion as they were found to be stable under reduction, as seen from temperature-programmed reduction studies.

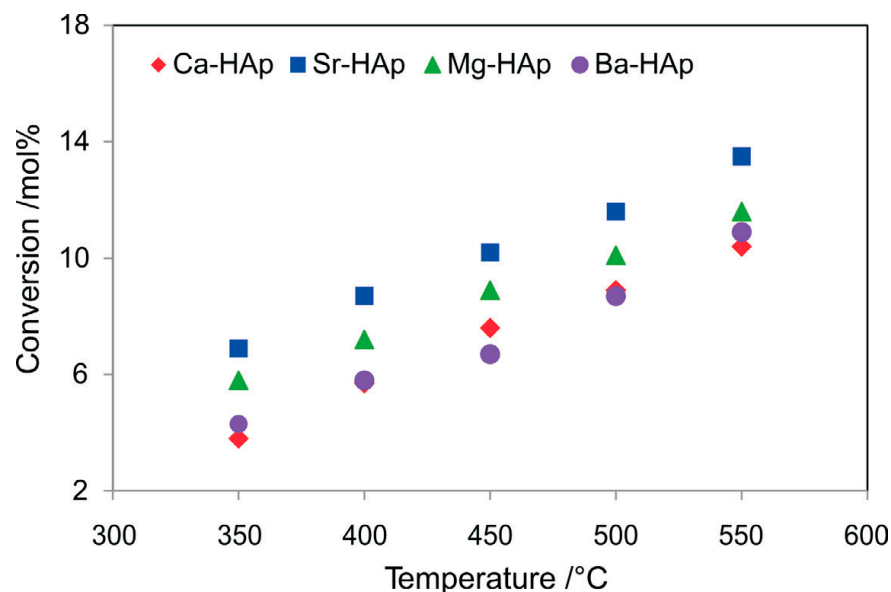


**Figure 10.** The effect of temperature on *n*-octane conversion over alkaline earth metal hydroxyapatites (GHSV = 4000 h<sup>-1</sup>, *n*-octane-to-oxygen molar ratio of 1:1). Reproduced from [56].

Figure 11 shows the product selectivity over the HAp catalysts. The cracked products composed mainly of ethane, propane and butane, while oxygenates were mainly C8 compounds such as octanal, octanol, 2-octanal and 2-octanol. The high selectivity to carbon oxides was attributed to the Bronsted acidity of the catalysts. Octenes had the highest selectivity amongst the ODH products, with *cis*- and *trans*-2-octenes being the most dominant. Their formation was also attributed to the presence of the metal in the HAp as well as Bronsted acidity [24]. The aromatic products were mainly *o*-xylene, ethylbenzene and styrene, and these were said to form via a cyclization mechanism of the octenes.

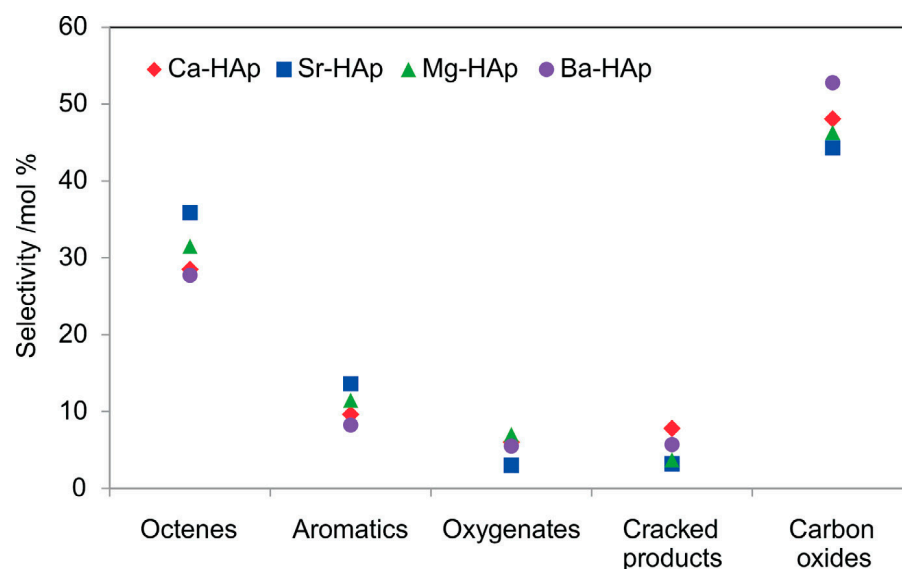


**Figure 11.** Product selectivity in the oxidative dehydrogenation of *n*-octane over alkaline earth metal hydroxyapatite catalysts at an iso-conversion of 8% (GHSV = 3700–4250 h<sup>-1</sup>, *n*-octane-to-oxygen molar ratio of 1:1, temperature = 500 °C). Reproduced from [56].

Farahani et al. [65] investigated the use of niobium-doped NiAl<sub>2</sub>O<sub>4</sub> catalysts in the oxidative dehydrogenation of *n*-octane. Niobium was chosen due to its ability to act as a high- and low-valence dopant and its ability to modify nickel-based materials by

decreasing the number of positive holes, as was observed in the oxidative dehydrogenation of ethane [66,67].  $\text{NiAl}_2\text{O}_4$  spinels with niobium loadings of 0.02, 0.06 and 0.10 were synthesized and tested over a temperature range of 450–550 °C. The C:O ratio chosen was 8:1 as it has been previously reported that conditions that are more anaerobic are suitable for the oxidative dehydrogenation of medium-chained alkanes [68]. In Figure 12, it can be seen that the octane conversion increased with increasing temperature over the niobium catalysts, whilst the undoped catalyst reached maximum conversion at 500 °C. This was reported to be due to coke deposition as observed from TGA data. It was also noted that the conversion decreased with increasing niobium loading.

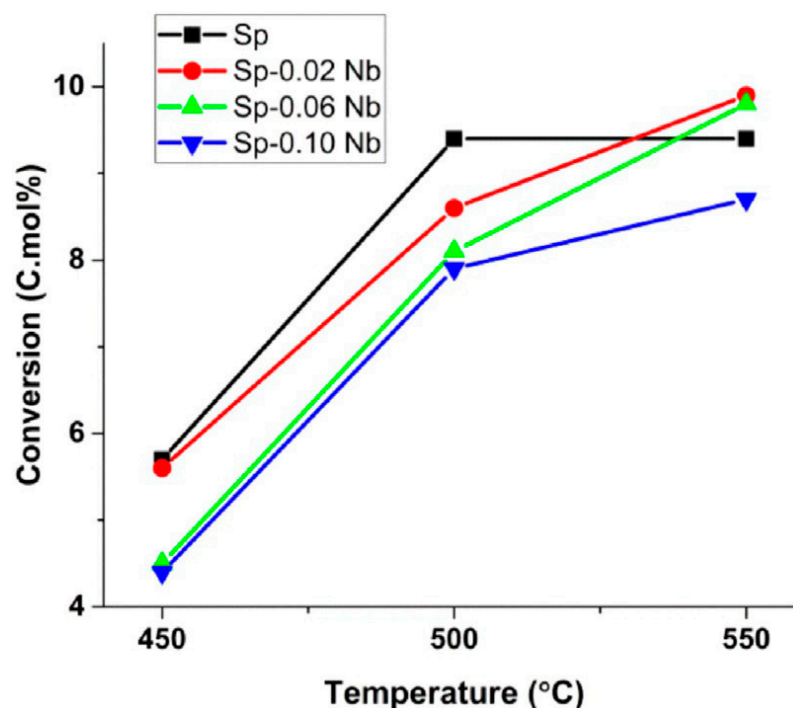


**Figure 12.** Catalytic conversion of *n*-octane over SP-*x* Nb (*x*: 0, 0.02, 0.06 and 0.10) catalysts. (Reaction conditions: C:O = 8:1, GHSV = 12,000 h<sup>-1</sup>, concentration of *n*-octane in the feed = 11%). Reproduced from [65]. © 2018 Wiley-VCH Verlag GmbH & Co. KGaA, Weinheim.

Figure 13 shows the selectivity to the products obtained over the catalysts at 450–550 °C. The selectivity to octenes decreased with a subsequent increase in aromatics and cracked products as the temperature increased, as octenes were precursors to these products. The selectivity to octenes decreased with increasing niobium loading, with the exception of the 0.02% Nb catalyst, while the selectivity to aromatics increased with decreasing niobium loading, with the exception of the 0.06% Nb catalyst. There was a direct correlation between the pore volumes and the aromatics selectivity. The selectivity to the cracked products was associated with the acidity of the catalysts which causes olefin cracking [69]. The surface acidity, which was believed to result when Nb substituted the octahedral Ni sites in the spinels forming a  $\text{NiNb}_2\text{O}_6$  complex, had inconclusive results which were out of the scope of the study. It would be beneficial if this complex could be synthesized and then tested in the ODH of *n*-octane to perhaps provide some insight into its properties and behavior in this reaction. The selectivity to carbon oxides decreased with increasing temperature, with the trend following the order of niobium substitution in the octahedral and tetrahedral sites of the spinels. The catalyst which was determined to have the lowest nickel occupation in both these sites (Sp-0.06 Nb) and less oxygen vacancies from XPS data showed the highest selectivity to carbon oxides.

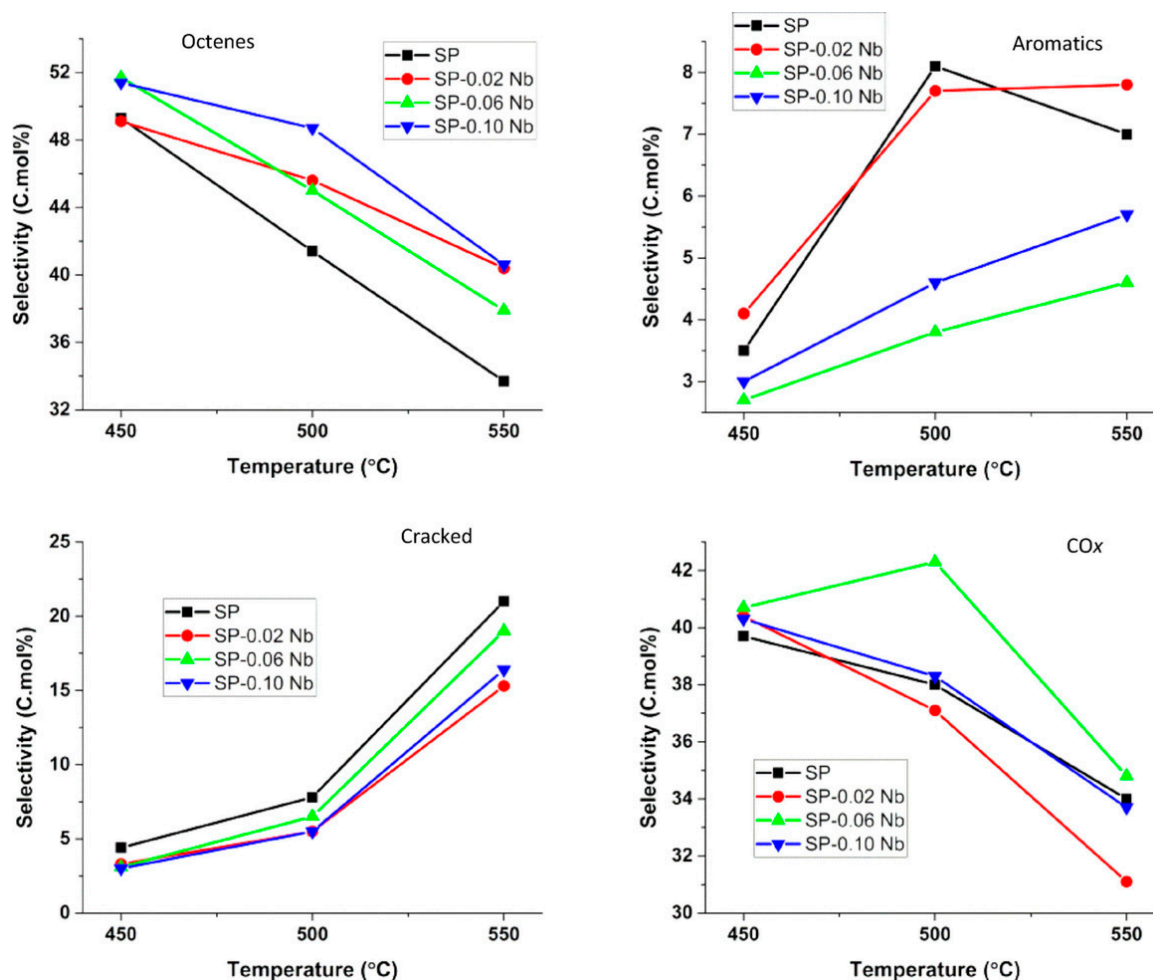


**Figure 13.** Selectivity to different products over SP-x Nb (x: 0, 0.02, 0.06 and 0.10) catalysts. (Reaction conditions: C:O = 8:1, GHSV = 12,000 h<sup>-1</sup>, concentration of *n*-octane in the feed = 11%). Reproduced from [65]. © 2018 Wiley-VCH Verlag GmbH & Co. KGaA, Weinheim.

Fadalla et al. [58] again reported the oxidative dehydrogenation of *n*-octane over molybdate-based catalysts. This study focused on the application of magnesium molybdate with different Mg:Mo ratios ranging from 1:0.87 to 1:1.25. After investigating the physicochemical properties of the bulk as well as the surfaces of the fresh and used catalysts, three active sites with different functionalities were identified. They deduced that the reduced molybdenum oxide (Mo<sup>4+</sup> and Mo<sup>5+</sup>) sites were responsible for dehydrogenation, whereas MgO (involved in the MgMoO<sub>4</sub> lattice or as the MgO phase) modified the density of basic sites that strongly controlled the adsorption of *n*-octane. The acidic sites which are thought to arise from molybdenum oxides promoted cracking and played an indirect role in increasing coke deposition over these materials.

Figure 14 shows the conversion and selectivity to the various products over the various MgMo catalysts. An increase in Mg content was seen to favor the catalysts' activity, with the catalyst with the highest Mg:Mo ratio deactivating the fastest. This catalyst, however, showed the highest selectivity to octenes and aromatics and the lowest selectivity to cracked products. Figure 15 shows the yield to primary, secondary and tertiary products over the various MgMo catalysts. Generally, an increase in catalyst acidity promotes olefin cracking in the dehydrogenation of paraffins. However, in this case, this was seen to occur with increasing basicity (increasing Mg content). The aromatics generally increased with increasing Mg content as a result of the formed olefins undergoing a cyclization mechanism. The cracked products, on the other hand, decreased with increasing Mg content.

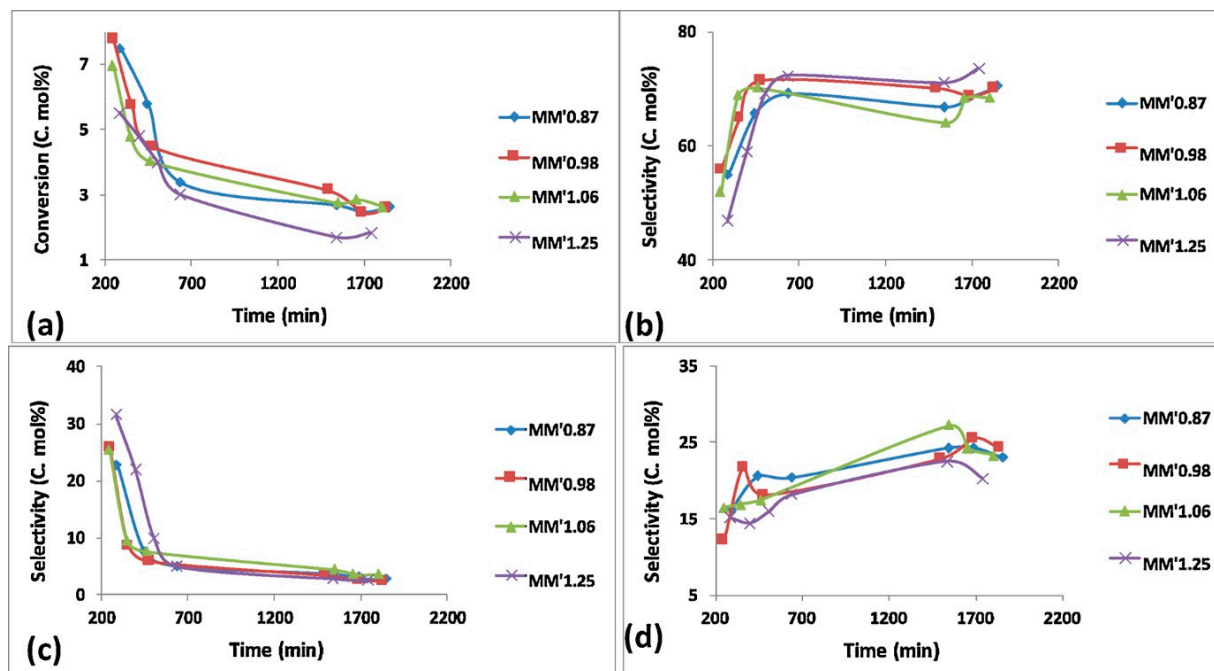


**Figure 14.** Catalytic results for MgMo catalysts: (a) conversion, (b) selectivity to octene isomers, (c) selectivity to aromatics, (d) selectivity to cracked products. (Reaction conditions: temperature = 550 °C, GHSV = 11,000 h<sup>-1</sup> and *n*-octane concentration in the feed = 11.5%). Reproduced from [58], ©2018 with permission from Elsevier.

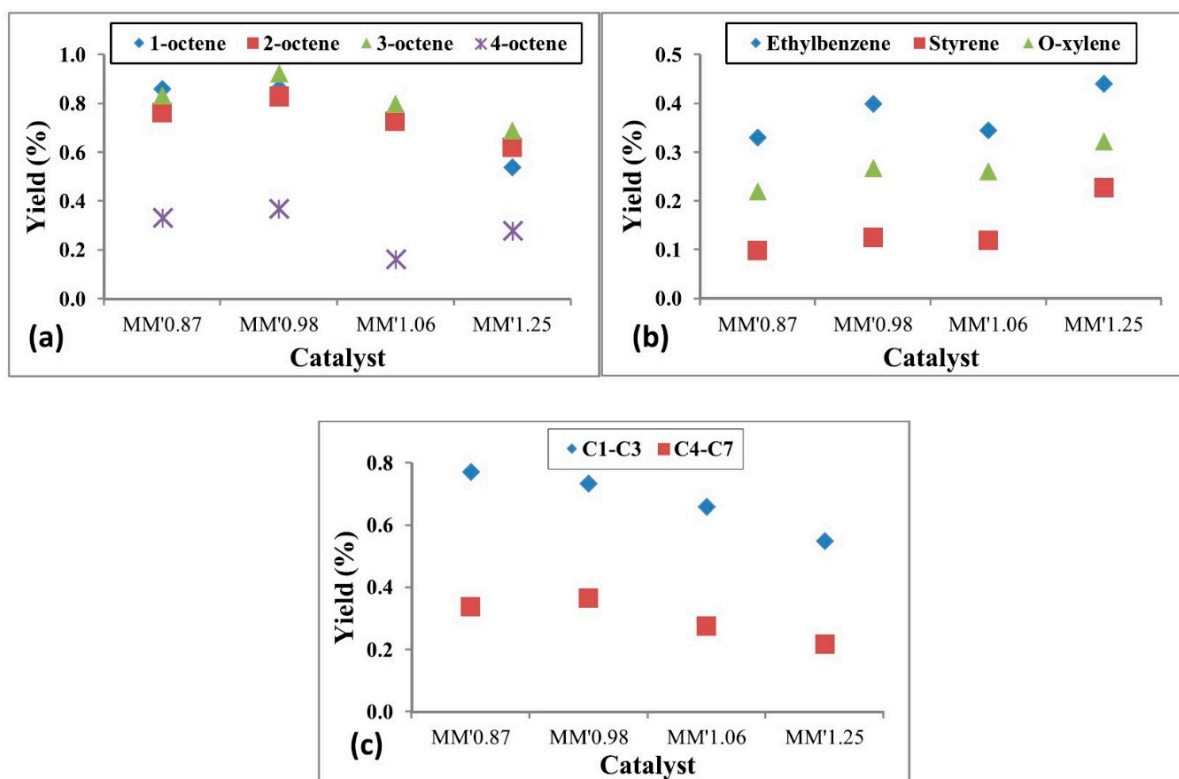


**Figure 15.** Yield to primary, secondary and tertiary products: (a) yield to octene isomers, (b) yield to aromatic products, (c) yield to cracked products. (Reaction conditions: temperature = 550 °C, GHSV = 11,000 h<sup>-1</sup> and *n*-octane concentration in the feed = 11.5%). Reproduced from [58], ©2018 with permission from Elsevier.

Bandaru et al. [70], on the other hand, looked at chromium-based molybdate catalysts where the Cr:Mo ratio varied from 0.4 to 1.3. They compared their findings by also looking at  $\text{MoO}_3$  and  $\text{Cr}_2\text{O}_3$  as catalysts. There was a steady increase in octane conversion with increasing temperature as the Cr content increased. The metal oxides ( $\text{MoO}_3$  and  $\text{Cr}_2\text{O}_3$ ) showed low conversion, and this was attributed to their low surface area.  $\text{MoO}_3$  gave the highest selectivity to octenes at 350 °C, which was then observed to decrease with increasing Cr content up to a ratio of 0.5. Catalysts with a higher Cr content were more selective to octene isomers at higher temperatures. It was concluded that to optimize octene selectivity above 450 °C, it is important to have a Cr/Mo ratio higher than that of pure chromium molybdate. Cracked products, which were reported to form via thermal and oxidative cracking [56,71], formed from a temperature of 400 °C. Their selectivity increased with increasing Cr content, with the highest selectivity being observed over  $\text{Cr}_2\text{O}_3$ . The aromatics (styrene, ethyl benzene, and o-xylene) formed from a temperature of 450 °C and increased with increasing temperature.

Padayachee et al. [45] investigated a range of transition metal oxide catalysts and their tendency to form carbon oxides in the ODH of *n*-octane. The reactions were carried at an iso-conversion of 10 mol% and a temperature of 450 °C, and a summary of their findings are shown in Figures 16 and 17. Moving across the first-row transition metal oxides from Ti to Cu,  $\text{TiO}_2$  showed the lowest selectivity to carbon oxides and the highest selectivity to octene isomers, which were desired, and a trend was observed when moving to  $\text{CuO}$ . As the octene isomers were the major products over all catalysts, it was concluded that they contributed to the formation of carbon oxides. The selectivity to carbon oxides increased with increasing  $\text{O}_2$  conversion, and it was suggested that there was a correlation between  $\text{O}_2$  activation and transformation on the metal oxide surface and the carbon oxides selectivity.

When looking closely at the 1-octene and internal octene selectivities (Figure 17), it was seen that the selectivity to 1-octene decreased from  $\text{TiO}_2$  to  $\text{CuO}$ , except over  $\text{ZnO}$ , and a similar trend was observed for the internal octene isomers. Overall, the selectivity to 1-octene was not favored over the investigated catalysts. However, it was reported that increasing space velocities and the C:O ratio could enhance the selectivity.

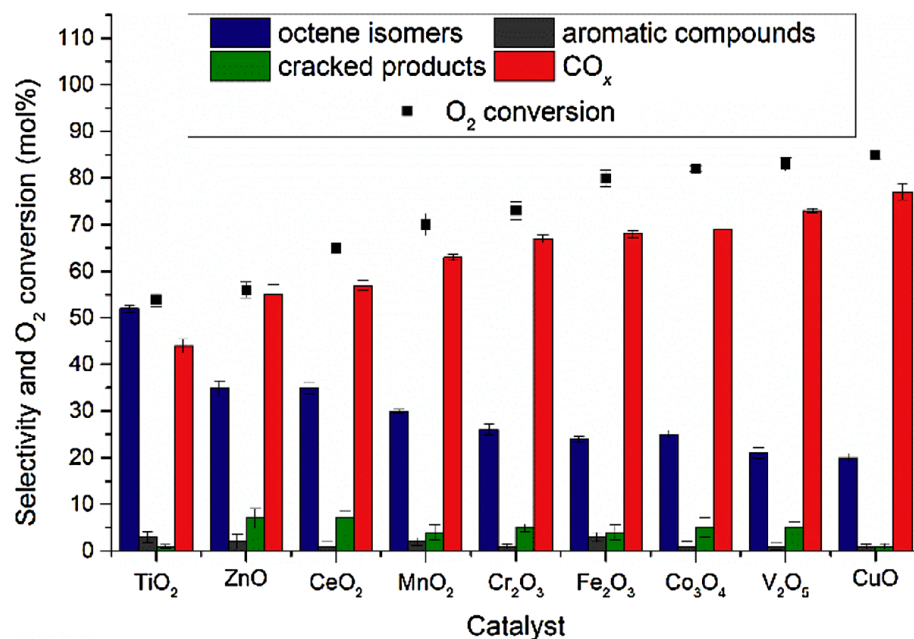


**Figure 16.** Catalytic data observed for the selected metal oxide catalysts at an iso-conversion of 10 mol%, tested at 450 °C, a C:O of 8:2 and varied GHSV. Reproduced from [45] ©2019, with permission from Elsevier.

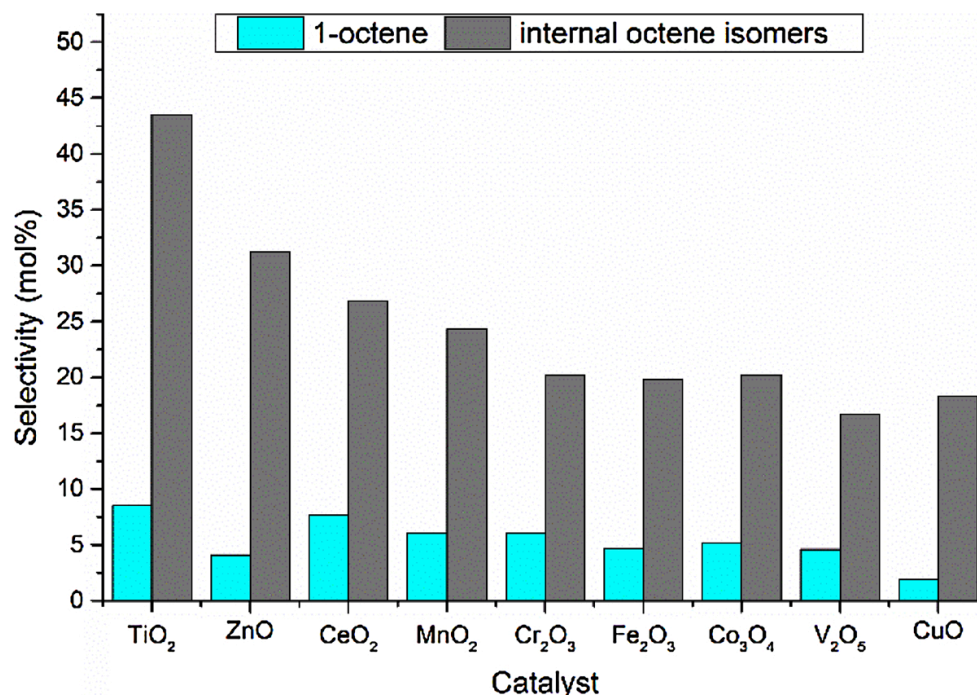


**Figure 17.** Octene isomer selectivity breakdown at iso-conversion (10 mol%). Reproduced from [45] ©2019, with permission from Elsevier.

#### 4.2. Supported Metal Oxides

The active sites in ODH are oxygen species that can be tailored by selecting the correct metal oxides and supports. The catalysts for these reactions are typically supported metal oxides with properties such as acid–base sites, redox sites and defect sites [72]. These materials have high surface area, porosity, and mechanical and thermal stability with various pore sizes, and these are known mostly as chemically inert materials. It has also been demonstrated that the performance of metal oxide catalysts is affected by properties related to defects, such as atom vacancies stepped edges, kinks, planar defects, as well as the electronic and geometric structure associated with these defects [22,73,74].

##### 4.2.1. Acid–Base Properties

It is generally accepted that during a reaction, an acid surface favors desorption of an acid intermediate, while a basic surface favors desorption of basic intermediates. This, in turn, avoids further over-oxidation of the adsorbed intermediate to CO<sub>2</sub>. Surface acid–base properties of the supports or isolated cations which are capable of activating C H bonds in the ODH of alkanes are important. Hence, the use of supports with varying acid–base properties is an advantage. Several authors have demonstrated how these sites play a role in the ODH of *n*-octane. An example is a study by Padayachee et al., where iron-modified hydroxyapatites were used for the ODH of *n*-octane. The results of this study showed that weak acidic sites favored adsorption of the *n*-octane molecules. The presence of moderate acid sites seemed to have led to the formation of ODH products, that is, octane isomers. This was followed by cracking or combustion, due to the strong interaction between the basic octene isomers formed on the surface of the catalyst [75]. Ntola et al. used V<sub>2</sub>O<sub>5</sub>/MgO catalysts with both acidic and basic properties. The catalyst that showed superior catalytic performance (due to a variety of properties) also showed weaker surface acidity which promoted higher selectivity to olefinic products. This was compared to the sample that had stronger acidity which resulted in the formation of CO<sub>x</sub> [52]. On the other hand, a study of boron- and barium-doped V/MgO catalysts related the low acidity of barium-doped V/MgO to the lowest activity and highest selectivity to carbon oxides [16].

Gaxiola et al. investigated the use of mesoporous silica SBA-15 doped with magnesium to avoid the leaching of the structure. The incorporated magnesium was thought to preserve the basic character, and these catalysts were applied in the oxidative dehydrogenation of *n*-octane. The incorporation of magnesium resulted in a better catalytic performance, compared to the SBA-15. This was ascribed to the magnesium metallic species on the surface of the catalyst, and the coordination environment around the active metal in this catalyst influenced the selectivity toward ODH products [32]. Several other authors have demonstrated the relationship between the acid–base properties of supported metal oxides and the activity and selectivity in the activation of *n*-octane [16,17,30,31,48,49,76].

#### 4.2.2. Redox Properties

The redox properties of metal oxide catalysts have also been reported to influence activity and selectivity in the ODH of intermediate alkanes. This relates to the property of metal oxides of being able to be reduced and re-oxidised easily [22,77]. The mechanism by which this occurs is described in details in the Section 3 [78]. Researchers have revealed how the redox properties of metal oxides affect catalytic performance in the ODH of *n*-octane.

Bugler [78] used molybdate catalysts denoted as  $AMoO_4$ , where A represented iron, cobalt or nickel in the oxidation state of +2 for the oxidative dehydrogenation of *n*-octane. An analysis of the product selectivity suggested that the conversion of *n*-octane to octenes was facilitated by the lattice oxygen from the iron molybdate catalysts or the bulk  $Mo_4O_{11}$  phase. They also found that nickel and cobalt molybdate catalysts, in which molybdenum was added in excess, performed better. Naicker et al. [79] discussed the redox properties of  $MnO_x/SBA-15$  catalysts for the activation of *n*-octane. Temperature-programmed reduction studies revealed that the catalysts could be reduced and re-oxidized easily to form MnO and  $Mn_3O_4$ . This suggested that these phases could be established with varying reduction and oxidation environments during a catalytic reaction. The results also demonstrated that  $MnO_2$  will form  $Mn_3O_4$  under the set redox conditions of the analysis. There are a number of authors who have attributed either an increase in the *n*-octane conversion or selectivity to the desired products to the catalysts' reducibility and re-oxidation properties [31,43,52,55].

Table 2 summarizes the catalytic results from the literature for the ODH of *n*-octane over supported metal oxide catalysts. It is evident that for the same catalytic system, different properties can be achieved depending on the catalyst synthesis method applied. Subsequently, different catalytic results can be obtained. This is one aspect that has not been fully explored in terms of the tailoring of the active sites using different synthesis methods.

**Table 2.** Product profiles from supported metal oxide catalysts.

Catalyst	Oxidant	Temperature/°C	C:Oxidant Ratio	Octane:O <sub>2</sub> Ratio	Conversion/%	Octenes/%	Aromatics/%	CO <sub>x</sub> /%	Reference
V/MgO	O <sub>2</sub>	350–550	-	0.1–1.6	11.5–58.8	6.9–49.4	9.9–20.5	25.3–78	[16]
Ba-V/MgO	O <sub>2</sub>	350–550	-	0.1–1.6	10.7–35.3	16.9–50.6	9.6–17.2	26.1–67.1	[16]
B-V/MgO	O <sub>2</sub>	350–550	-	0.1–1.6	11–43.7	9.7–50	9.8–19	24.8–76	[16]
4 wt% VO <sub>x</sub> /TiO <sub>2</sub>	CO <sub>2</sub>	550	8:7.5	-	5	68	10	-	[30]
9 wt% VO <sub>x</sub> /TiO <sub>2</sub>	CO <sub>2</sub>	550	8:7.5	-	3	75	6	-	[30]
V/MgO_1*	O <sub>2</sub>	350–550	-	0.8	1.7–17	36–43	10–16	38–40	[47]
V/MgO_2*	O <sub>2</sub>	350–550	-	0.8	3–21	32–38	11–19	30–48	[47]
V/MgO_3*	O <sub>2</sub>	350–550	-	0.8	2–19	37–38	10–14	35–45	[47]
V/MgO	O <sub>2</sub>	350–550	-	0.8	2–22	41–43	17–18	31–39	[49]
B-V/MgO	O <sub>2</sub>	350–550	-	0.8	2–17	40–50	6–12	32–45	[49]
Ba-V/MgO	O <sub>2</sub>	350–550	-	0.8	2–23	40–48	1–20	30–38	[49]
4wt%MnO <sub>x</sub> /SBA-15	O <sub>2</sub>	450	8:3	-	9.8	32	5	45	[50]

Table 2. Cont.

Catalyst	Oxidant	Temperature/°C	C:Oxidant Ratio	Octane:O <sub>2</sub> Ratio	Conversion/%	Octenes/%	Aromatics/%	CO <sub>x</sub> /%	Reference
7wt% MnO <sub>x</sub> /SBA-15	O <sub>2</sub>	450	8:3	-	5	27	10	37	[50]
10wt% MnO <sub>x</sub> /SBA-15	O <sub>2</sub>	450	8:3	-	3	27	8	46	[50]
18wt% MnO <sub>x</sub> /SBA-15	O <sub>2</sub>	450	8:3	-	2	16	6	48	[50]
VO <sub>x</sub> /MgO (citric acid) <sup>@</sup>	O <sub>2</sub>	400	8:2	-	9	34	2	64	[52]
VO <sub>x</sub> /MgO (oxalylhydrazide) <sup>@</sup>	O <sub>2</sub>	400	8:2	-	13	53	5	36	[52]
VO <sub>x</sub> /MgO (hydrazine hydrate) <sup>@</sup>	O <sub>2</sub>	400	8:2	-	10	44	2	44	[52]
VO <sub>x</sub> /MgO (glycine) <sup>@</sup>	O <sub>2</sub>	400	8:2	-	15	65	5	27	[52]
VO <sub>x</sub> /MgO (urea) <sup>@</sup>	O <sub>2</sub>	400	8:2	-	16	57	18	33	[52]
5%V/Sr-HAp	O <sub>2</sub>	350–550	-	1:1	16–28	68–75	10–14	10–13	[76]
7.5%V/Sr-HAp	O <sub>2</sub>	350–550	-	1:1	20–38	48–69	12–25	15–17	[76]
15%V/Sr-HAp	O <sub>2</sub>	350–550	-	1:1	24–46	40–62	20–33	13–15	[76]
2wt% MnO <sub>x</sub> /SBA-15 <sup>#</sup>	O <sub>2</sub>	450	8:2	-	-	12	5	75	[79]
9wt% MnO <sub>x</sub> /SBA-15 <sup>#</sup>	O <sub>2</sub>	450	8:2	-	-	28	1	70	[79]
18wt% MnO <sub>x</sub> /SBA-15 <sup>#</sup>	O <sub>2</sub>	450	8:2	-	-	26	3	72	[79]
2wt% MnO <sub>x</sub> /SBA-15 <sup>§</sup>	O <sub>2</sub>	450	8:2	-	-	17	3	80	[79]
9wt% MnO <sub>x</sub> /SBA-15 <sup>§</sup>	O <sub>2</sub>	450	8:2	-	-	38	4	55	[79]
18wt% MnO <sub>x</sub> /SBA-15 <sup>§</sup>	O <sub>2</sub>	450	8:2	-	-	36	4	57	[79]

\* MgO support was prepared via three different methods. <sup>@</sup> In parentheses is the fuel used during solution combustion synthesis. <sup>#</sup> Prepared via deposition–precipitation. <sup>§</sup> Prepared via wet impregnation.

#### 4.2.3. The Effect of Catalyst Synthesis Methods

For practical and realistic applications of the oxidative activation of alkanes, selectivity remains the key parameter in terms of improving energy and raw material utilization efficiency and CO<sub>2</sub> reduction. This implies that there is a need to control parameters such as the nature of active sites, reaction mechanisms and reactant composition. One of the ways to go about this is to consider how catalyst synthesis methods influence the active

centers required to increase selectivity towards ODH products and reduce CO<sub>2</sub> formation. For the ODH and CO<sub>2</sub>-ODH of *n*-octane, a variety of catalyst synthesis methods have been explored. These include wet impregnation, precipitation and solution combustion synthesis. The following section discusses a variety of chosen catalysts, prepared using different synthesis methods.

#### Wet Impregnation

Elkhalifa et al. [47] prepared three V/MgO catalysts following the wet impregnation method. The catalysts were synthesized using different MgO precursors. The authors noted that altering synthesis parameters led to the formation of catalysts with different textural properties, morphology and acidity. As a result, the catalytic performances were different. The selectivity to aromatics and CO<sub>x</sub> varied with the different MgO precursors. Figure 18 shows a decrease in CO<sub>x</sub> selectivity between 350 and 450 °C and an increase at temperatures between 500 and 550 °C. This indicates a contribution from the secondary combustion of the formed aromatics to the CO<sub>x</sub> selectivity. This was attributed to two of the catalysts displaying relatively higher surface acidity. For vanadia-based catalysts, the selectivity is said to be influenced by the acid–base character of the catalyst's surface [80].

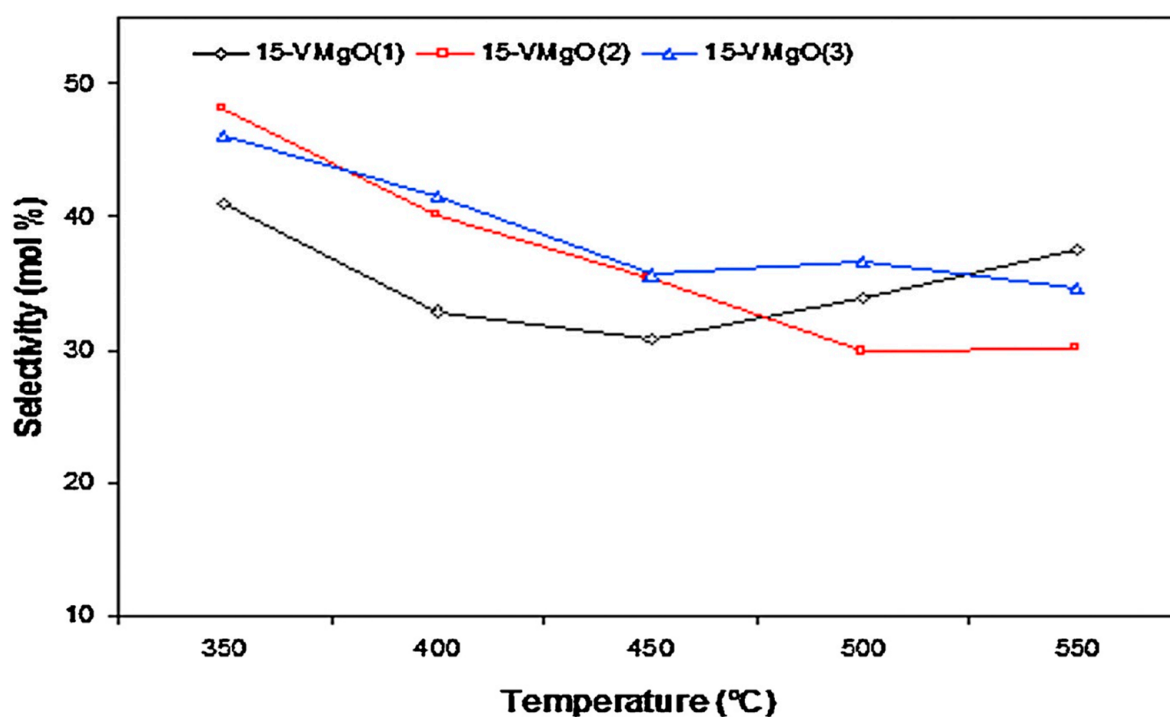


**Figure 18.** Selectivity to CO<sub>x</sub> over V/MgO catalysts at 350–550 °C and GHSV of 8000 h<sup>-1</sup>. Reproduced from [47] ©2019, with permission from Elsevier.

In another study, Elkhalifa et al. [49] used the wet impregnation method to synthesize V/MgO catalysts. However, the catalysts were doped with barium and boron. The dopants induced changes in the catalysts' properties, such as the reducibility and acid–base character. As a consequence, there were notable changes in the catalytic performances. The barium dopant increased the styrene selectivity and yield, while doping with boron rather adversely affected the activity and the ODH selectivity of the V/MgO catalysts. The undoped catalyst displayed the highest selectivity to octenes, while the Ba-doped V/MgO showed lower selectivities. For aromatics formation, the undoped and Ba-doped V/MgO catalysts showed comparable values, whereas the B-V/MgO catalyst displayed the lowest. This is due to the acid–base characters of the doped catalysts. A short residence time was expected for the octenes, which are basic, on the surface of the Ba-V/MgO catalyst due to its low acidity.

Adam et al. [31] synthesized Cr-Fe catalysts supported on  $\text{MgAl}_2\text{O}_4$  for the  $\text{CO}_2$ -dehydrogenation of *n*-octane via wet impregnation. The catalyst support, which was a  $\text{MgAl}_2\text{O}_4$  spinel, was prepared following the sol-gel auto-combustion method. The authors noted physical and chemical properties that could be attributed to the synthesis method. For instance, the vacuum impregnation method contributed to maintaining the surface area of the support by increasing the dispersion of the active metals and/or preventing the loaded metal oxide particles from sitting at the mouth of the pore openings. Further to this, the supported catalysts demonstrated notable amounts of strong basic sites, which are required for  $\text{CO}_2$  adsorption and activation during the ODH process. From Figure 19, it can be observed that the 2Cr-Fe catalyst had a higher number of C8 products. The higher and stable selectivity to C8 products observed over this catalyst is reflected in the higher surface basicity of the catalyst and lower carbon deposition.

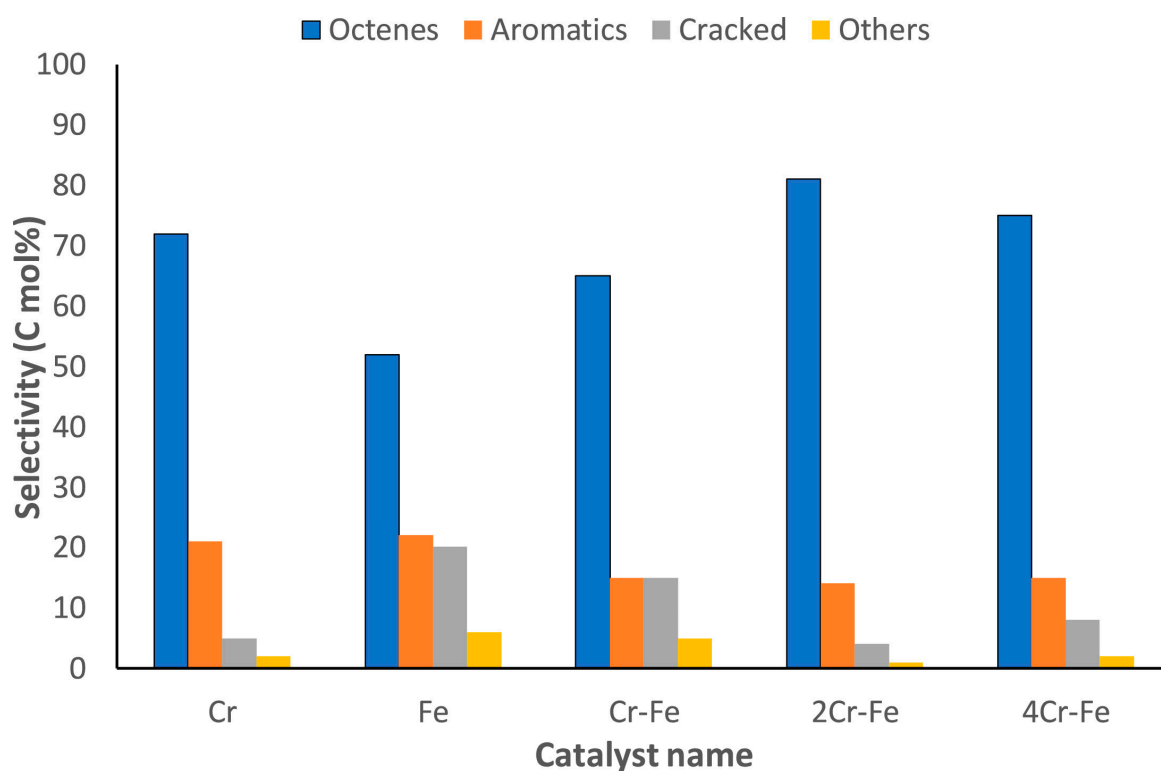


**Figure 19.** Products selectivity at iso-conversion of ca. 5% after 12 h time on stream, tested at 500 °C,  $\text{CO}_2$ /octane ratio 2:1, GHSV 6000–10,000  $\text{h}^{-1}$ . Reproduced from [31] ©2019, with permission from Elsevier.

#### Solution Combustion Synthesis

The same VMgO catalytic system was studied by Ntola et al. [52,72] for the ODH of *n*-octane, using solution combustion synthesis. In this study, five different fuels were used, viz., glycine, citric acid, urea, oxalyldihydrazide and hydrazine hydrate. The use of different fuels as reducers resulted in the creation of defects and different redox and basic properties. Catalysts that displayed an easy reduction of  $\text{V}^{5+}$  to  $\text{V}^{4+}$  also demonstrated better octane conversion and selectivity to C8 products. Minor defects on the MgO surface of the highly performing catalyst were observed, which was also consistent with the catalyst's strong basicity. Figure 20 shows the selectivity profiles of the five catalysts synthesized using different fuels. The high selectivity to C8 products (65%) over the GLY catalyst and the subsequent low selectivity to  $\text{CO}_x$  was due to the short residence time of the products on the catalyst surface. The authors also noted that vanadium speciation, oxygen vacancies and surface basicity were significantly more important than the surface vanadium concentration in giving high selectivity to octenes.

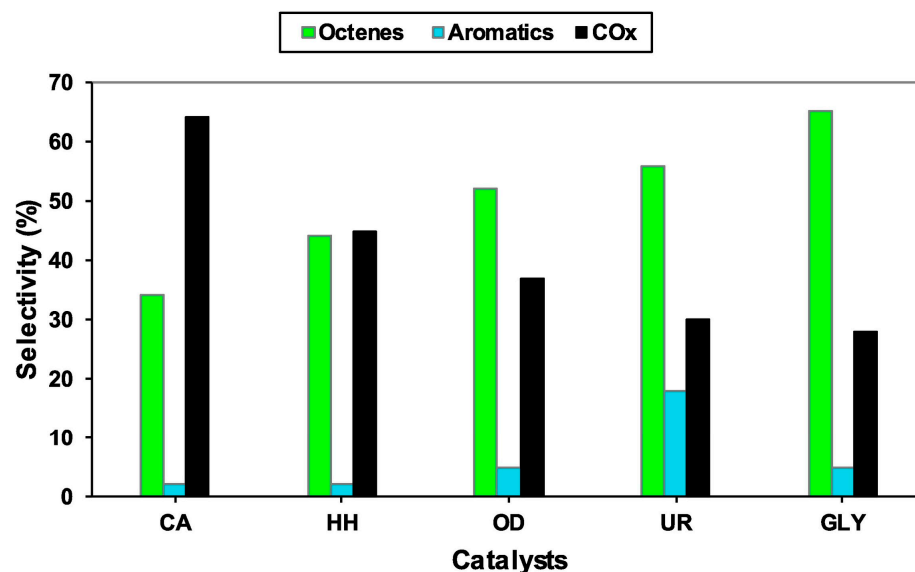


**Figure 20.** Selectivity at iso-conversion (~9%) of the VO<sub>x</sub>/MgO catalysts tested at 400 °C, feed = 5% *n*-octane, C:O: 8:2. Reproduced from [52] ©2019, with permission from Elsevier.

### Precipitation

Manganese oxide catalysts with varying weight loadings, supported on SBA-15, were synthesized by Naicker et al. [79] for the oxidative dehydrogenation of *n*-octane. Two synthesis methods were used to prepare the catalysts, viz., wet impregnation and deposition-precipitation. The characterization results demonstrated that the two groups of catalysts differed in particle size and dispersion, which subsequently led to diverse catalytic results. The results in the selectivity profiles of the catalysts prepared via both wet impregnation and deposition-precipitation showed that catalysts prepared via wet impregnation exhibited better selectivities towards octene isomers compared to the catalysts prepared via deposition-precipitation at iso-conversion. This was ascribed to greater accessibility to the active site for the 9W (9%wt prepared via wet impregnation) catalysts when compared to the 9D (9%wt prepared via deposition-precipitation) catalysts. Greater accessibility permitted an enhanced interaction between the *n*-octane and the metal oxide. Similarly, octene isomer selectivity increased for the 2 wt% catalysts compared to the support. These catalysts had particle sizes between 20 and 30 nm. This effect was more prominent when comparing the 9 wt% catalysts and the support. The Mn<sub>3</sub>O<sub>4</sub> particle size for the 9 wt% catalysts and 2 wt% catalysts were in a similar range (20–30 nm). The octene isomer selectivity increased for the higher loading mainly due to the higher metal content. For the 18 wt% catalysts, the particle sizes were significantly larger, and this resulted in decreased selectivities towards octene isomers when compared to the 9 wt% catalysts. This suggested that the key for this metal oxide and support system would be maintaining a higher metal content with a metal oxide particle size of 20–30 nm.

### 5. Perspectives

ODH transformation is still a challenging task due to the low intrinsic chemical reactivity of the alkanes, which demands a high energy input to activate them. Activating a longer chain hydrocarbon makes the task even more challenging, as long-chain alkane reactions are limited mainly to combustion and cracking due to the C single-bond H bond being non-polar; this results in the formation of radicals through cracking. One of the main challenges is minimizing the formation of carbon oxides, which is an environmental issue, vs. product selectivity. Amongst the factors that influence the formation of CO<sub>x</sub>/total oxidation products is temperature. Low-temperature active catalysts would be key in avoiding total-oxidation products, due to the fact that an equilibrium conversion of alkanes is known to increase with temperature, while selectivity to alkenes decreases with increasing

temperature and chain length. However, this must be conducted in conjunction with pressure adjustments. Mostly, ODH reactions operate at ambient pressures. A slight increase in pressure to allow a decrease in temperature could alleviate the situation.

Despite supported and unsupported metal oxides having been the main catalysts used in the ODH of *n*-octane, newly used catalysts include the family of zeolites. Even though zeolites are mainly acidic material that would facilitate mostly the adsorption of *n*-octane, and do not follow the proposed MvK mechanism, a lot of room exists for the modification of acid sites to attain sufficient basicity for desorption of the desired products. This includes, for instance, the use of alkali metals as dopants during synthesis for the modification of acidity and reducibility. It is generally difficult to find a metal oxide system with a combination of all the desired properties, that is, surface acidity, the extent of reduction and bandgap energy. A compromise often has to be reached between high alkane conversions and selectivity to the desired products. Even though the literature has reported on different catalytic performances when catalyst synthesis methods are varied, this is one aspect that has not been fully explored in terms of the tailoring of the active sites using different synthesis methods.

Some of these difficulties may also be associated with a lack of understanding for the usually proposed mechanisms for the ODH of *n*-octane. The identification of intermediate products and examination of particular/specific reaction routes plays a role on the selectivity to desired products. This includes, for instance, determining the rate-determining step in a sequence of consecutive reactions. Also, very little attention is given to the reaction kinetics which may be influenced by internal diffusion processes. In addition, coke deposition on the (internal) catalytic surface, which leads to a decay of the catalyst activity with time, has not been studied sufficiently for *n*-octane ODH.

## 6. Conclusions

Due to the increased demand for alkenes, aromatic compounds and functionalized alkanes, both industrially and scientifically, there has been a need to convert medium- and long-chain alkanes. While this review is limited to the ODH of *n*-octane, we discuss how alkenes are produced via the dehydrogenation of alkanes industrially, which is an endothermic process that operates at high temperatures, resulting in high energy consumption. This necessitates research toward the use of oxidants, hence the ODH route with lower energy demand than the non-oxidative route. Despite the advantages of ODH, we highlight challenges associated with the use of oxidants such as O<sub>2</sub> and CO<sub>2</sub>. This review discusses in detail how these two oxidants are used and their dissociation mechanisms. Further to this, we discuss the mechanisms in which alkane oxidation is proposed to occur, which are the Mars Van Krevelen, Langmuir–Hinshelwood and Eley–Rideal mechanisms. The limitation of the Mars Van Krevelen is that it was developed for oxidation reactions based on transition metal oxides catalysts which can easily change their oxidation states. While different catalytic systems have been employed for the conversion of *n*-octane to value-added products, we limit this review to supported, unsupported and mixed metal oxides, with a slight mention of zeolite materials. Unsupported catalysts include hydrotalcite-like catalysts, cobalt substituted ceria, hydroxyapatites, niobium-doped NiAl<sub>2</sub>O<sub>4</sub>, catalysts, molybdate-based catalysts, chromium-based molybdate and a range of chromium oxide catalysts. For supported catalysts, we focus on MgO-supported vanadia, (synthesized using various methods), MnO<sub>x</sub>/SBA-15, VO<sub>x</sub>/TiO<sub>2</sub> and V/Sr-HAp. We also demonstrate that different properties can be achieved using different catalyst synthesis methods for the same material. We discuss how the choice of catalyst affects *n*-octane conversion and product selectivity profiles particularly between 300 and 500 °C. In all the catalytic systems, the difficulty to suppress the formation of carbon oxides is common.

**Author Contributions:** Conceptualization, P.N. and M.S.; methodology, P.N. and M.S.; formal analysis, P.N. and M.S.; investigation, P.N. and M.S.; resources, P.N. and M.S.; data curation, P.N. and M.S.; writing—original draft preparation, P.N. and M.S.; writing—review and editing, P.N. and M.S. All authors have read and agreed to the published version of the manuscript.

**Funding:** This research received no funding.

**Data Availability Statement:** Data reported were taken from publications included in the references.

**Conflicts of Interest:** The authors declare no conflicts of interest.

## References

1. Dhar, A.; Vekariya, R.L.; Bhadja, P. *n*-Alkane isomerization by catalysis—A method of industrial importance: An overview. *Cogent Chem.* **2018**, *4*, 1514686. [[CrossRef](#)]
2. Anderson, J.; Wells, R.; Galadima, A.; Ibrahim, B. Solid acid catalysts in heterogeneous *n*-alkanes hydroisomerisation for increasing octane number of gasoline. *Afr. Sci.* **2021**, *11*, 53–61.
3. Budweg, S.; Junge, K.; Beller, M. Catalytic oxidations by dehydrogenation of alkanes, alcohols and amines with defined (non)-noble metal pincer complexes. *Catal. Sci. Technol.* **2020**, *10*, 3825–3842. [[CrossRef](#)]
4. Wu, L.; Fleischer, I.; Jackstell, R.; Profir, I.; Franke, R.; Beller, M. Ruthenium-catalyzed hydroformylation/reduction of olefins to alcohols: Extending the scope to internal alkenes. *J. Am. Chem. Soc.* **2013**, *135*, 14306–14312. [[CrossRef](#)] [[PubMed](#)]
5. Jeske, K.; Rösler, T.; Belleflamme, M.; Rodenas, T.; Fischer, N.; Claeys, M.; Leitner, W.; Vorholt, A.J.; Prieto, G. Direct conversion of syngas to higher alcohols via tandem integration of Fischer–Tropsch synthesis and reductive hydroformylation. *Angew. Chem.* **2022**, *134*, e202201004. [[CrossRef](#)]
6. Yin, M.; Natelson, R.H.; Campos, A.A.; Kolar, P.; Roberts, W.L. Aromatization of *n*-octane over Pd/C catalysts. *Fuel* **2013**, *103*, 408–413. [[CrossRef](#)]
7. Lappin, G. *Alpha Olefins Applications Handbook*; CRC Press: Boca Raton, FL, USA, 2014.
8. Hájeková, E.; Špodová, L.; Bajus, M.; Mlynková, B. Separation and characterization of products from thermal cracking of individual and mixed polyalkenes. *Chem. Pap.* **2007**, *61*, 262–270. [[CrossRef](#)]
9. Derouane, E.G.; Haber, J.; Lemos, F.; Ribeiro, F.R.; Guisnet, M. *Catalytic Activation and Functionalisation of Light Alkanes: Advances and Challenges*; Springer: Berlin/Heidelberg, Germany, 2013.
10. Asinger, F. *Paraffins: Chemistry and Technology*; Elsevier: Amsterdam, The Netherlands, 2016.
11. Nawaz, Z. Light alkane dehydrogenation to light olefin technologies: A comprehensive review. *Rev. Chem. Eng.* **2015**, *31*, 413–436. [[CrossRef](#)]
12. Gambo, Y.; Adamu, S.; Tanimu, G.; Abdullahi, I.M.; Lucky, R.A.; Ba-Shammakh, M.S.; Hossain, M.M. CO<sub>2</sub>-mediated oxidative dehydrogenation of light alkanes to olefins: Advances and perspectives in catalyst design and process improvement. *Appl. Catal. A Gen.* **2021**, *623*, 118273. [[CrossRef](#)]
13. Sarathy, S.M.; Yeung, C.; Westbrook, C.K.; Pitz, W.J.; Mehl, M.; Thomson, M.J. An experimental and kinetic modeling study of *n*-octane and 2-methylheptane in an opposed-flow diffusion flame. *Combust. Flame* **2011**, *158*, 1277–1287. [[CrossRef](#)]
14. Széchenyi, A.; Solymosi, F. *n*-Octane aromatization on Mo<sub>2</sub>C-containing catalysts. *Appl. Catal. A Gen.* **2006**, *306*, 149–158. [[CrossRef](#)]
15. Hone, C.A.; Kappe, C.O. The use of molecular oxygen for liquid phase aerobic oxidations in continuous flow. *Acc. Sustain. Flow Chem.* **2020**, *377*, 67–110.
16. Elkhalifa, E.A.; Friedrich, H.B. Dehydrocyclization of *n*-octane over boron-and barium-doped V-Mg-O catalysts: Influence of *n*-octane/oxygen ratios. *Appl. Petrochem. Res.* **2017**, *7*, 23–32. [[CrossRef](#)]
17. Farahani, M.D.; Fadlalla, M.I.; Ezekiel, I.P.; Osman, N.S.; Moyo, T.; Claeys, M.; Friedrich, H.B. Nb<sub>2</sub>O<sub>5</sub> as a radical modulator during oxidative dehydrogenation and as a Lewis acid promoter in CO<sub>2</sub> assisted dehydrogenation of octane over confined 2D engineered NiO–Nb<sub>2</sub>O<sub>5</sub>–Al<sub>2</sub>O<sub>3</sub>. *Catal. Sci. Technol.* **2021**, *11*, 5321–5334. [[CrossRef](#)]
18. Westbrook, C.K.; Pitz, W.J.; Herbinet, O.; Curran, H.J.; Silke, E.J. A comprehensive detailed chemical kinetic reaction mechanism for combustion of *n*-alkane hydrocarbons from *n*-octane to *n*-hexadecane. *Combust. Flame* **2009**, *156*, 181–199. [[CrossRef](#)]
19. Oehlschlaeger, M.A.; Steinberg, J.; Westbrook, C.K.; Pitz, W.J. The autoignition of iso-cetane at high to moderate temperatures and elevated pressures: Shock tube experiments and kinetic modeling. *Combust. Flame* **2009**, *156*, 2165–2172. [[CrossRef](#)]
20. Isazade, A.F. A short overview on oxidation of *n*-alkanes on various catalysts and C–H bond activation. *Process. Petrochem. Oil Refin.* **2022**, *23*, 99.
21. Dasireddy, V.D.B.C. Oxidation and Oxidative Dehydrogenation of *n*-Octane Using V<sub>2</sub>O<sub>5</sub> Supported on Hydroxyapatites. Ph.D. Thesis, University of KwaZulu-Natal, Durban, South Africa, 2012.
22. Védrine, J.C.; Fehete, I. Heterogeneous partial oxidation catalysis on metal oxides. *Comptes Rendus Chim.* **2016**, *19*, 1203–1225. [[CrossRef](#)]
23. Ruiz, P.; Karelovic, A.; Cortés Corberán, V. Unconventional oxidants for gas-phase oxidations. In *Handbook of Advanced Methods and Processes in Oxidation Catalysis: From Laboratory to Industry*; World Scientific: Singapore, 2014; pp. 877–920.
24. Dasireddy, V.D.; Singh, S.; Friedrich, H.B. Activation of *n*-octane using vanadium oxide supported on alkaline earth hydroxyapatites. *Appl. Catal. A Gen.* **2013**, *456*, 105–117. [[CrossRef](#)]
25. Boreskov, G. Forms of oxygen bonds on the surface of oxidation catalysts. *Discuss. Faraday Soc.* **1966**, *41*, 263–276. [[CrossRef](#)]
26. Carley, A.F.; Davies, P.R.; Roberts, M.W. Activation of oxygen at metal surfaces. *Philos. Trans. R. Soc. A Math. Phys. Eng. Sci.* **2005**, *363*, 829–846. [[CrossRef](#)]

27. Fadlalla, M.I.; Friedrich, H.B. The effect of the oxidation environment on the activity and selectivity to aromatics and octenes over cobalt molybdate in the oxidative dehydrogenation of *n*-octane. *Catal. Sci. Technol.* **2014**, *4*, 4378–4385. [[CrossRef](#)]
28. Liu, P.; Zhang, L.; Li, M.; Sun, N.; Wei, W. Recent progress in Cr-based catalysts for oxidative dehydrogenation of light alkanes by employing CO<sub>2</sub> as a soft oxidant. *Clean Energy* **2021**, *5*, 623–633. [[CrossRef](#)]
29. Coleman, M.G.; Brown, A.N.; Bolton, B.A.; Guan, H. Iron-catalyzed Oppenauer-type oxidation of alcohols. *Adv. Synth. Catal.* **2010**, *352*, 967–970. [[CrossRef](#)]
30. Moloi, S.; Farahani, M.D.; Mahomed, A.S.; Singh, S.; Friedrich, H.B. The role of monomeric VO<sub>x</sub> supported on anatase in catalytic dehydrogenation of *n*-octane assisted by CO<sub>2</sub> addition. *Mol. Catal.* **2022**, *530*, 112578. [[CrossRef](#)]
31. Adam, D.S.; Mahomed, A.S.; Bala, M.D.; Friedrich, H.B. The role of CO<sub>2</sub> in the dehydrogenation of *n*-octane using Cr-Fe catalysts supported on MgAl<sub>2</sub>O<sub>4</sub>. *Mol. Catal.* **2021**, *513*, 111782. [[CrossRef](#)]
32. Gaxiola, E.; Castellón, F.; Hernández, J.A.; Acosta, B.; Díaz de León, J.; Fuentes, S.; Zepeda, T. Oxidative dehydrogenation of *n*-octane over Mg-containing SBA-15 material. *Mater. Res. Innov.* **2018**, *22*, 247–253. [[CrossRef](#)]
33. Yao, S.; Yan, B.; Jiang, Z.; Liu, Z.; Wu, Q.; Lee, J.H.; Chen, J.G. Combining CO<sub>2</sub> reduction with ethane oxidative dehydrogenation by oxygen-modification of molybdenum carbide. *ACS Catal.* **2018**, *8*, 5374–5381. [[CrossRef](#)]
34. Huš, M.; Kopač, D.; Bajec, D.; Likozar, B. Effect of surface oxidation on oxidative propane dehydrogenation over chromia: An ab initio multiscale kinetic study. *ACS Catal.* **2021**, *11*, 11233–11247. [[CrossRef](#)] [[PubMed](#)]
35. Dasireddy, V.D.; Huš, M.; Likozar, B. Effect of O<sub>2</sub>, CO<sub>2</sub> and N<sub>2</sub>O on Ni–Mo/Al<sub>2</sub>O<sub>3</sub> catalyst oxygen mobility in *n*-butane activation and conversion to 1,3-butadiene. *Catal. Sci. Technol.* **2017**, *7*, 3291–3302. [[CrossRef](#)]
36. Mars, P.; van Krevelen, D.W. Oxidations carried out by means of vanadium oxide catalysts. *Chem. Eng. Sci.* **1954**, *3*, 41–59. [[CrossRef](#)]
37. Védrine, J.C. Heterogeneous Partial (amm)Oxidation and Oxidative Dehydrogenation Catalysis on Mixed Metal Oxides. *Catalysts* **2016**, *6*, 22. [[CrossRef](#)]
38. Hosono, Y.; Saito, H.; Higo, T.; Watanabe, K.; Ito, K.; Tsuneki, H.; Maeda, S.; Hashimoto, K.; Sekine, Y. Co–CeO<sub>2</sub> Interaction Induces the Mars–van Krevelen Mechanism in Dehydrogenation of Ethane. *J. Phys. Chem. C* **2021**, *125*, 11411–11418. [[CrossRef](#)]
39. Pan, Z.-Z.; Li, Y.; Zhao, Y.; Zhang, C.; Chen, H. Bulk phase charge transfer in focus—And in sequential along with surface steps. *Catal. Today* **2021**, *364*, 2–6. [[CrossRef](#)]
40. Liang, R.; Hu, A.; Hatat-Fraile, M.; Zhou, N. Fundamentals on Adsorption, Membrane Filtration, and Advanced Oxidation Processes for Water Treatment. In *Nanotechnology for Water Treatment and Purification*; Hu, A., Apblett, A., Eds.; Springer International Publishing: Cham, Switzerland, 2014; pp. 1–45.
41. Baxter, R.J.; Hu, P. Insight into why the Langmuir–Hinshelwood mechanism is generally preferred. *J. Chem. Phys.* **2002**, *116*, 4379–4381. [[CrossRef](#)]
42. Mahata, A.; Nair, A.S.; Pathak, B. Recent advancements in Pt-nanostructure-based electrocatalysts for the oxygen reduction reaction. *Catal. Sci. Technol.* **2019**, *9*, 4835–4863. [[CrossRef](#)]
43. Dasireddy, V.D.; Khan, F.B.; Bharuth-Ram, K.; Singh, S.; Friedrich, H.B. Non oxidative and oxidative dehydrogenation of *n*-octane using FePO<sub>4</sub>: Effect of different FePO<sub>4</sub> phases on the product selectivity. *Catal. Sci. Technol.* **2020**, *10*, 7591–7600. [[CrossRef](#)]
44. Elkhalfifa, E.A.; Friedrich, H.B. Magnesium oxide as a catalyst for the dehydrogenation of *n*-octane. *Arab. J. Chem.* **2018**, *11*, 1154–1159. [[CrossRef](#)]
45. Padayachee, D.; Mahomed, A.S.; Singh, S.; Friedrich, H.B. Selected metal oxides for CH bond activation of *n*-octane and propensity for CO<sub>x</sub> formation: An empirical study. *Mol. Catal.* **2019**, *464*, 1–9. [[CrossRef](#)]
46. Padayachee, D.; Mahomed, A.S.; Singh, S.; Friedrich, H.B. Effect of the TiO<sub>2</sub> anatase/rutile ratio and interface for the oxidative activation of *n*-octane. *ACS Catal.* **2020**, *10*, 2211–2220. [[CrossRef](#)]
47. Elkhalfifa, E.A.; Friedrich, H.B. Oxidative dehydrogenation and aromatization of *n*-octane over VMgO catalysts obtained by using different MgO precursors and different precursor treatments. *J. Mol. Catal. A Chem.* **2014**, *392*, 22–30. [[CrossRef](#)]
48. Gounden, N. The Oxidative Activation of *n*-Octane over Titania Supported Cobalt Catalysts. Ph.D. Thesis, University of KwaZulu-Natal, Durban, South Africa, 2013.
49. Elkhalfifa, E.; Friedrich, H. Effects of boron and barium dopants on VMgO catalysts employed in the oxidative dehydrogenation of *n*-octane. *Kinet. Catal.* **2015**, *56*, 212–221. [[CrossRef](#)]
50. Golandaj, A.J.; Mahomed, A.S.; Singh, S.; Friedrich, H.B. Effect of different weight loadings of MoO<sub>x</sub>/SBA-15 on the oxidative dehydrogenation of *n*-octane. *J. Porous Mater.* **2015**, *22*, 787–796. [[CrossRef](#)]
51. Elkhalfifa, E.A.; Friedrich, H.B. Oxidative dehydrogenation of *n*-octane over a vanadium–magnesium oxide catalyst: Influence of the gas hourly space velocity. *Arab. J. Chem.* **2019**, *12*, 2464–2469. [[CrossRef](#)]
52. Ntola, P.; Friedrich, H.B.; Singh, S.; Olivier, E.J.; Farahani, M.; Mahomed, A.S. Effect of the fuel on the surface VO<sub>x</sub> concentration, speciation and physico-chemical characteristics of solution combustion synthesised VO<sub>x</sub>/MgO catalysts for *n*-octane activation. *Catal. Commun.* **2023**, *174*, 106571. [[CrossRef](#)]
53. Ndelela, S.S.; Friedrich, H.B.; Cele, M.N. Oxidative dehydrogenation of *n*-octane using Ba and Ga-modified faujasite type catalysts prepared by different methods. *J. Porous Mater.* **2021**, *28*, 593–603. [[CrossRef](#)]
54. Yeo, B.R. Alkanes, Alkenes and Aromatics: The Oxidative Dehydrogenation of *n*-Octane Using Iron Molybdate Catalysts. Ph.D. Thesis, Cardiff University, Cardiff, Wales, 2014.

55. Dasireddy, V.D.; Friedrich, H.B.; Singh, S. Studies towards a mechanistic insight into the activation of *n*-octane using vanadium supported on alkaline earth metal hydroxyapatites. *Appl. Catal. A Gen.* **2013**, *467*, 142–153. [[CrossRef](#)]
56. Dasireddy, V.D.; Friedrich, H.B.; Singh, S. A kinetic insight into the activation of *n*-octane with alkaline-earth metal hydroxyapatites. *S. Afr. J. Chem.* **2015**, *68*, 195–200. [[CrossRef](#)]
57. Padayachee, D. The Catalysed Activation of *n*-Octane over Iron Modified Hydroxyapatites. Ph.D. Thesis, University of KwaZulu-Natal, Durban, South Africa, 2014.
58. Fadlalla, M.I.; Farahani, M.D.; Friedrich, H.B. Three inter-linked active sites in the dehydrogenation of *n*-octane over magnesium molybdate based catalysts and their influences on coking and cracking side reactions. *Mol. Catal.* **2018**, *461*, 86–96. [[CrossRef](#)]
59. Furukawa, S.; Shishido, T.; Teramura, K.; Tanaka, T. Reaction mechanism of selective photooxidation of hydrocarbons over Nb<sub>2</sub>O<sub>5</sub>. *J. Phys. Chem. C* **2011**, *115*, 19320–19327. [[CrossRef](#)]
60. Friedrich, H.B.; Mahomed, A.S. The oxidative dehydrogenation of *n*-octane to styrene using catalysts derived from hydrotalcite-like precursors. *Appl. Catal. A Gen.* **2008**, *347*, 11–22. [[CrossRef](#)]
61. Narayanappa, M.; Dasireddy, V.D.B.C.; Friedrich, H.B. Catalytic oxidation of *n*-octane over cobalt substituted ceria (Ce<sub>0.90</sub>Co<sub>0.10</sub>O<sub>2-δ</sub>) catalysts. *Appl. Catal. A Gen.* **2012**, *447–448*, 135–143. [[CrossRef](#)]
62. Sugiyama, S.; Osaka, T.; Hirata, Y.; Sotowa, K.-I. Enhancement of the activity for oxidative dehydrogenation of propane on calcium hydroxyapatite substituted with vanadate. *Appl. Catal. A Gen.* **2006**, *312*, 52–58. [[CrossRef](#)]
63. Monma, H. Catalytic behavior of calcium phosphates for decompositions of 2-propanol and ethanol. *J. Catal.* **1982**, *75*, 200–203. [[CrossRef](#)]
64. Sugiyama, S.; Osaka, T.; Ueno, Y.; Sotowa, K.-I. Oxidative Dehydrogenation of Propane over Vanadate Catalysts Supported on Calcium and Strontium Hydroxyapatites. *J. Jpn. Pet. Inst.* **2008**, *51*, 50–57. [[CrossRef](#)]
65. Farahani, M.D.; Dasireddy, V.D.B.C.; Friedrich, H.B. Oxidative Dehydrogenation of *n*-Octane over Niobium-Doped NiAl<sub>2</sub>O<sub>4</sub>: An Example of Beneficial Coking in Catalysis over Spinel. *ChemCatChem* **2018**, *10*, 2059–2069. [[CrossRef](#)]
66. Sun, X.; Li, B.; Metiu, H. Ethane Activation by Nb-Doped NiO. *J. Phys. Chem. C* **2013**, *117*, 23597–23608. [[CrossRef](#)]
67. Popescu, I.; Skoufa, Z.; Heracleous, E.; Lemonidou, A.; Marcu, I.-C. A study by electrical conductivity measurements of the semiconductive and redox properties of Nb-doped NiO catalysts in correlation with the oxidative dehydrogenation of ethane. *Phys. Chem. Chem. Phys.* **2015**, *17*, 8138–8147. [[CrossRef](#)]
68. Zhang, J.; Liu, X.; Blume, R.; Zhang, A.; Schlögl, R.; Su, D.S. Surface-Modified Carbon Nanotubes Catalyze Oxidative Dehydrogenation of *n*-Butane. *Science* **2008**, *322*, 73–77. [[CrossRef](#)]
69. Sattler, J.J.H.B.; Ruiz-Martinez, J.; Santillan-Jimenez, E.; Weckhuysen, B.M. Catalytic Dehydrogenation of Light Alkanes on Metals and Metal Oxides. *Chem. Rev.* **2014**, *114*, 10613–10653. [[CrossRef](#)]
70. Bandaru, H.; Mahomed, A.S.; Singh, S.; Friedrich, H.B. The effect of varying the metal ratio in a chromium molybdate catalysts for the oxidative dehydrogenation of *n*-octane. *Mol. Catal.* **2018**, *460*, 74–82. [[CrossRef](#)]
71. Goncharov, D.V.; Belyaevskii, M.Y. Analysis and Mathematical Description of the Thermal-Oxidative Cracking of Naphtha. *Chem. Pet. Eng.* **2005**, *41*, 193–198. [[CrossRef](#)]
72. Ntola, P.; Friedrich, H.B.; Mahomed, A.S.; Olivier, E.J.; Govender, A.; Singh, S. Exploring the role of fuel on the microstructure of VOx/MgO powders prepared using solution combustion synthesis. *Mater. Chem. Phys.* **2022**, *278*, 125602. [[CrossRef](#)]
73. Zhou, Y.; Chai, Y.; Li, X.; Wu, Z.; Lin, J.; Han, Y.; Li, L.; Qi, H.; Gu, Y.; Kang, L. Defect-rich TiO<sub>2</sub> in situ evolved from MXene for the enhanced oxidative dehydrogenation of ethane to ethylene. *ACS Catal.* **2021**, *11*, 15223–15233. [[CrossRef](#)]
74. Stoian, M.; Rogé, V.; Lazar, L.; Maurer, T.; Védrine, J.C.; Marcu, I.-C.; Fechet, I. Total oxidation of methane on oxide and mixed oxide ceria-containing catalysts. *Catalysts* **2021**, *11*, 427. [[CrossRef](#)]
75. Padayachee, D.; Dasireddy, V.D.; Singh, S.; Friedrich, H.B.; Bharuth-Ram, K.; Govender, A. An investigation of iron modified hydroxyapatites used in the activation of *n*-octane. *Mol. Catal.* **2017**, *438*, 256–266. [[CrossRef](#)]
76. Dasireddy, V.D.; Singh, S.; Friedrich, H.B. Vanadium oxide supported on non-stoichiometric strontium hydroxyapatite catalysts for the oxidative dehydrogenation of *n*-octane. *J. Mol. Catal. A Chem.* **2014**, *395*, 398–408. [[CrossRef](#)]
77. Grant, J.T.; Venegas, J.M.; McDermott, W.P.; Hermans, I. Aerobic oxidations of light alkanes over solid metal oxide catalysts. *Chem. Rev.* **2017**, *118*, 2769–2815. [[CrossRef](#)]
78. Bugler, K. The Catalytic Oxidative Dehydrogenation of *n*-Octane Over Iron and Other Metal Molybdates. Ph.D. Thesis, Cardiff University, Cardiff, Wales, 2017.
79. Naicker, K.; Mahomed, A.S.; Friedrich, H.B.; Singh, S. Influence of preparation method of high surface area MnOx/SBA-15 catalysts for the activation of *n*-octane. *J. Porous Mater.* **2019**, *26*, 301–309. [[CrossRef](#)]
80. Blasco, T.; Nieto, J.L.; Dejoz, A.; Vazquez, M. Influence of the acid-base character of supported vanadium catalysts on their catalytic properties for the oxidative dehydrogenation of *n*-butane. *J. Catal.* **1995**, *157*, 271–282. [[CrossRef](#)]

**Disclaimer/Publisher's Note:** The statements, opinions and data contained in all publications are solely those of the individual author(s) and contributor(s) and not of MDPI and/or the editor(s). MDPI and/or the editor(s) disclaim responsibility for any injury to people or property resulting from any ideas, methods, instructions or products referred to in the content.